The oncoprotein DEK affects the outcome of PARP1/2 inhibition during replication stress

Magdalena Ganz[1¶], Christopher Vogel[1¶], Christina Czada[1], Vera Jörke[1], Rebecca Kleiner[1], Agnieszka Pierzynska-Mach[2,3], Francesca Cella Zanacchi[2,4], Alberto Diaspro[2,5], Ferdinand Kappes[6], Alexander Bürkle[7], and Elisa Ferrando-May[1*]

[1]Department of Biology, Bioimaging Center, University of Konstanz, Konstanz, Germany

[2]Nanoscopy and NIC@IIT, Istituto Italiano di Tecnologia, Genoa, Italy

[3]Department of Experimental Oncology, European Institute of Oncology, Milan, Italy

[4]Biophysics Institute (IBF), National Research Council (CNR), Genoa, Italy

[5]DIFILAB, Department of Physics, University of Genoa, Genoa, Italy

[6]Xi'an Jiaotong-Liverpool University, Dushu Lake Higher Education Town, Suzhou, China

[7]Department of Biology, Molecular Toxicology Group, University of Konstanz, Konstanz, Germany

Short title: DEK and PARP in replication stress

* Corresponding author

email: elisa.may@uni-konstanz.de

¶These authors contributed equally to this work

ABSTRACT

DNA replication stress is a major source of genomic instability and is closely linked to tumor formation and progression. Poly(ADP-ribose)polymerases1/2 (PARP1/2) enzymes are activated in response to replication stress resulting in poly(ADP-ribose) (PAR) synthesis. PARylation plays an important role in the remodelling and repair of impaired replication forks, providing a rationale for targeting highly replicative cancer cells with PARP1/2 inhibitors. The human oncoprotein DEK is a unique, non-histone chromatin architectural protein whose deregulated expression is associated with the development of a wide variety of human cancers. Recently, we showed that DEK is a high-affinity target of PARylation and that it promotes the progression of impaired replication forks. Here, we investigated a potential functional link between PAR and DEK in the context of replication stress. Under conditions of mild replication stress induced either by topoisomerase1 inhibition with camptothecin or nucleotide depletion by hydroxyurea, we found that the effect of acute PARP1/2 inhibition on replication fork progression is dependent on DEK expression. Reducing DEK protein levels also overcomes the restart impairment of stalled forks provoked by blocking PARylation. Non-covalent DEK-PAR interaction via the central PAR-binding domain of DEK is crucial for counteracting PARP1/2 inhibition as shown for the formation of RPA positive foci in hydroxyurea treated cells. Finally, we show by iPOND and super resolved microscopy that DEK is not directly associated with the replisome since it binds to DNA at the stage of chromatin formation. Our report sheds new light on the still enigmatic molecular functions of DEK and suggests that DEK expression levels may influence the sensitivity of cancer cells to PARP1/2 inhibitors.

INTRODUCTION

Poly(ADP-ribosyl)ation (PARylation) is an abundant protein posttranslational modification regulating numerous cellular functions among which the maintenance of genomic stability plays a prominent role [1]. The enzyme responsible for 85-90% of the cellular PAR synthesis activity is PARP1, with PARP2 accounting for the remainder [2]. PAR can be covalently linked to and/or interact non-covalently with target proteins. PARylation is highly dynamic and can be very transient in nature due to the activity of the de-modifying enzyme, the PAR glycohydrolase or PARG [3]. Inhibition of PARylation by small molecule compounds is a recently approved strategy for the treatment of ovarian cancer [4]. The rationale for the use of PARP1/2 inhibitors in chemotherapy is based on their synthetic lethal interaction with DNA damaging agents in cells which are deficient for recombinational DNA repair through mutations in BRCA1/2 [5, 6]. In these cells, inhibition of PARylation abrogates base excision repair thereby turning endogenous single strand breaks (SSBs) in highly toxic, non-repairable double strand breaks (DSBs). In addition, PARP1/2 inhibitors possess DNA trapping activity which causes DSBs on its own due to the collision of PARP-DNA complexes with the DNA replication and transcription machineries [7]. Impaired DNA replication has recently come into the focus as a further source of DNA lesions which can become lethal to cells treated with PARP1/2 inhibitors. If not removed timely, replication blocks lead to fork collapse leaving behind single ended DNA strand breaks as well as SSBs which require PARylation for their prompt repair. PARP1/2 was also shown to be directly involved in replication fork stabilization and protection. Thus, PARP is required for the restart of collapsed forks after prolonged exposure to hydroxyurea (HU) [8], protects transiently stalled forks from premature and extensive

71 resection [9] and regulates fork reversal induced e.g. by low doses of camptothecin
72 (CPT). More precisely, PARylation prevents RecQ helicase from resolving regressed
73 forks prematurely, thus avoiding fork run off across DNA lesions and DSB generation
74 [10, 11]. Finally, PARP1/2 was shown to play an important role also during
75 unperturbed DNA replication. Using pharmacological PARG inhibition to stabilize and
76 detect basal PAR levels, the polymer was shown to be required for sensing and
77 repairing a sub-set of unligated Okazaki fragments thus providing a back-up pathway
78 for the completion of lagging strand DNA synthesis [12].

79 DEK is a non-histone chromatin protein which is ubiquitously present in higher
80 eukaryotes [13]. Its binding to DNA is regulated by abundant post-translational
81 modifications, including phosphorylation [14, 15], acetylation [16, 17], and PARylation
82 [18-20]. Covalent PARylation of DEK is efficiently triggered by DNA damage leading
83 to the loss of its DNA binding and folding activities [20]. The DEK amino acid sequence
84 bears three PAR-binding motifs which mediate non-covalent PAR interaction *in vitro*,
85 thereby moderately reducing DNA binding but incrementing DEK multimerization [18].
86 A continuously increasing number of studies link DEK overexpression to cancer
87 development, pinpointing DEK as a “bona fide” oncogene [21]. DEK is considered a
88 potential therapeutic target and a biomarker for breast and ovarian cancer [22-24],
89 retinoblastoma [25], colorectal [26] and bladder cancer [27] as well as for melanoma
90 progression [28, 29]. DEK has a pleiotropic mode of action and can influence diverse
91 regulatory circuits in the cell, a notion supported also by the recent elucidation of its
92 interactome [30]. Downregulation of DEK expression increases the susceptibility to
93 DNA damage [20, 31], attenuates apoptosis [32] and senescence [21], and affects
94 proliferation and chemoresistance [23, 33, 34] . On the mechanistic level, DEK is
95 known to have DNA folding activity, principally via its ability to introduce positive

96 supercoils [35-37]. Thus, DEK has been involved in splicing [38], transcriptional
97 activation and repression, heterochromatin stability [39], DNA repair [40, 41] and DNA
98 replication [42, 43]. Concerning the latter, we recently proposed that DEK acts as a
99 tumour promoter by protecting cells from the deleterious consequences of DNA
100 replication stress. In particular, we showed that DEK facilitates replication fork
101 progression under stress, and counteracts DNA damage arising from impeded
102 replication as well as its transmission to daughter cells [43]. In this study, we set out
103 to examine a potential functional link between DEK and PARP1/2 in the context of
104 DNA replication stress. Our data reveal that for mildly stressed replication forks, the
105 consequences of PARP1/2 inhibition depend on DEK expression.
106

107 MATERIAL AND METHODS

108 Cell culture

109 U2-OS osteosarcoma cells were cultured in McCoy's 5a modified medium (Thermo
110 Fisher Scientific) supplemented with 10 % fetal bovine serum (FCS; Capricorn
111 Scientific and PAA Laboratories), 100 U/ml penicillin and 100 µg/ml streptomycin (both
112 Thermo Fisher Scientific). U2-OS control and shDEK cells [43] were additionally
113 supplemented with 2 µg/ml puromycin (Merck). Puromycin was omitted 36 h prior to
114 experiments. U2-OS shDEK cells stably express an shRNA targeting the human DEK
115 transcript, resulting in a permanent reduction of DEK protein levels of around 90 %
116 [43]. U2-OS wildtype cells were a kind gift of G. Marra, University of Zurich,
117 Switzerland. To generate U2-OS GFP-DEK cells, the eGFP sequence has been
118 inserted at the 5`end of the endogenous DEK coding sequence in wildtype cells via
119 TALEN-mediated genome editing (Vogel et al., in preparation). HeLa S3 cervical

120 adenocarcinoma cells were cultured in DMEM medium (Thermo Fisher Scientific)
121 supplemented with 10 % fetal bovine serum, 100 U/ml penicillin, 100 µg/ml
122 streptomycin and 6 mM L-glutamine (Thermo Fisher Scientific). BJ-5ta foreskin
123 fibroblasts were cultured in a 4:1 mixture of DMEM medium and Medium 199 medium
124 (Thermo Fisher Scientific) supplemented with 10 % fetal bovine serum, 4 mM L-
125 glutamine and 10 µg/ml hygromycin B (Merck).
126 For induction of replication stress, cells were treated with hydroxyurea (HU; Merck)
127 or camptothecin (CPT; Merck) as indicated. PARP1/2 activity was inhibited with ABT-
128 888 or AZD-2281 (both Selleckchem) as indicated.
129

130 Isolation of Proteins on Nascent DNA (iPOND)

131 iPOND was performed as described by Sirbu et al. [44], with minor modifications. At
132 least $1x10^8$ HeLa S3 cells per sample were pulsed with 10 µM EdU (Thermo Fisher
133 Scientific) for the indicated times and either incubated with 10 µM thymidine (Merck)
134 for 0 - 30 min before fixation (chase experiments) or fixated immediately (pulse
135 experiments). For replication stress experiments thymidine containing medium was
136 supplemented with 2 mM HU and/or 1 µM ABT-888. Click reaction to label EdU-
137 containing DNA was performed using biotin-PEG3-azide (Jena Bioscience) for 90 min
138 and cells were sonicated in a Bioruptor sonicator (Diogenode) to solubilize chromatin
139 fragments. Biotin-linked fragments were precipitated overnight at 4 °C using
140 streptavidin-coupled magnetic beads (0.8 µm, Solulink). Chromatin bound proteins
141 ("Capture") were subjected to Western blot analysis using the following antibodies:
142 polyclonal rabbit α-DEK K-877 (1:20,000; [20]), monoclonal mouse α-PCNA (1:9,000;
143 PC10, Cell Signaling Technology), polyclonal rabbit α-H3 (1:150,000; ab1791, Abcam).
144

145 ## DNA fiber assay

146 For the determination of tract length ratios, U2-OS shDEK and control cells were
147 labelled with 60 µM CldU (Merck) for 20 min and subsequently treated with 250 µM
148 IdU (Merck) for 20 min in the presence or absence of 25 mM CPT and/or 1 µM ABT-
149 888 as indicated. For the analysis of replication fork restart, cells were labelled with 60
150 µM CldU for 20 min and subsequently treated with 4 mM HU and 60 µM CldU for 4 h.
151 After washing, cells were labelled with 250 µM IdU for 20 min in the presence or
152 absence of 1 µM ABT-888.

153 DNA fiber spreads were prepared as described by Merrick et al. [45] with
154 modifications: After trypsination and resuspension in ice-cold PBS, labelled and
155 unlabelled cells were mixed in a 1:5 ratio. 12.5 µl of the mixture were diluted with 7.5
156 µl lysis buffer (200 mM Tris-HCl pH 7.4, 50 mM EDTA, 0.5 % SDS) on a glass slide.
157 After 9 min the slides were tilted at 30-45° and the resulting DNA spreads were air-
158 dried and fixed overnight in a methanol:acetic acid mixture (3:1) at 4 °C. Following
159 denaturing and blocking with 2 % BSA in 0.1 % Tween 20, the slides were incubated
160 for 2.5 h with rat α-BrdU (1:200; BU1/75 (ICR1), Abcam; detects CldU) and mouse α-
161 BrdU (1:200; B44 from BD Biosciences; detects IdU) antibodies. Fibers were treated
162 with goat α-mouse AlexaFluor-488 and goat α-rat AlexaFluor-546 (both Thermo Fisher
163 Scientific) secondary antibodies for 1h at RT, allowed to air-dry and mounted in
164 ProLong Gold Antifade (Thermo Fisher Scientific). Widefield microscopy was
165 performed with a Zeiss Axio Observer Z1 equipped with a Plan Apochromat 63x/1.40
166 oil DIC objective lens. Data were evaluated using Fiji v1.49u (National Institutes of
167 Health, MD [46]) and the fiber tool of the BIC macro tool box [43].

168

169

170 **Selection of DEK-GFP expressing cells**

171 U2-OS shDEK cells were transfected with plasmids encoding DEK WT-GFP or DEK
172 PBD2-Mut2-GFP. After 24 h, cells were sorted using a FACSAria Illu (BD Biosciences).
173 Low DEK GFP expressing cells were collected in McCoy's 5a modified medium
174 supplemented with 20 % FCS. To determine expression levels of endogenous and
175 ectopic DEK, total proteins were extracted with SDS lysis buffer. Cleared lysates were
176 subjected to Western blotting with the following antibodies: polyclonal rabbit α-DEK K-
177 877 (1:20,000; [20]), polyclonal rabbit α-PCNA (1:5,000; ab18197, Abcam).

178

179 **Immunofluorescence**

180 For immunofluorescence detection of Rad51, U2-OS cells were preextracted using
181 CSK-buffer (10 mM Hepes-KOH pH 7.4, 300 mM sucrose, 100 mM NaCl, 3 mM MgCl2,
182 0.5 % Triton X-100, 10 mM NaF, 1 mM NaVO3, 11.5 mM Na-molybdat) for 5 min on
183 ice after treatment and fixed using 4 % PFA/PBS supplemented with 10 mM NaF and
184 1 mM NaVO3 (20 min, RT). For immunofluorescence detection of 53BP1, γH2AX and
185 RPA70, cells were fixed with 4 % PFA/PBS without preextraction. After
186 permeabilization, cells were incubated with primary antibodies diluted in 1 % BSA/PBS
187 (Rad51, 53BP1, γH2AX) or 10 % FBS/0.05 % Na-azide/culture medium (RPA70)
188 overnight at 4 °C. The following primary antibodies were used: polyclonal rabbit α-
189 53BP1 (1:200; H-300, Santa Cruz), monoclonal rabbit α-RPA70 (1:1000; ab79398,
190 Abcam), monoclonal mouse α-γH2AX (1:500; Ser139, clone JBW301, Santa Cruz),
191 polyclonal rabbit α-Rad51 (1:100; H-92, Santa Cruz). After washing with PBS, cells
192 were incubated with secondary antibodies diluted in 1 % BSA/PBS at RT for 1 h. The
193 following secondary antibodies were used: goat α-mouse AlexaFluor-488, goat α-

194 rabbit AlexaFluor-546 (both 1:400; both Thermo Fisher Scientific). For nuclear
195 counterstaining, cells were incubated in 200 ng/µl Hoechst 33342/PBS (Merck).
196 Coverslips were mounted on microscopy slides using Aqua Polymount (Polysciences).
197 Replicating cells were visualized by labelling with 10 µM EdU 10 min prior to replication
198 stress induction. Cells were fixed and immunostainings performed as described above.
199 After incubation with secondary antibodies, EdU was detected using the Klick-it EdU
200 Imaging Kit with AlexaFluor-488 or -647 azide (all Thermo Fisher Scientific) following
201 manufacturer´s instructions. Nuclear counterstaining and mounting of coverslips was
202 performed as described above.
203

204 Confocal and superresolution microscopy

205 Confocal microscopy was performed with a Zeiss LSM 510 Meta and a Zeiss LSM
206 780 equipped with a Plan Neofluar 40x/1.30 oil or a Plan Apochromat 40x/1.40 oil
207 objective lens, respectively. Image analysis was done with Fiji v1.49u [46] using the
208 ImageJ BIC macro tool box [43]. For counting DNA damage foci, appropriate noise
209 parameters for each channel were determined manually and applied to all samples
210 within one experiment. For the determination of the number of cells positive for lesion
211 markers, the lower threshold for the number of foci per nucleus was set such to include
212 95 % of untreated control cells. The threshold was applied to all samples within one
213 experiment. Cells exceeding the threshold were classified as positive for the
214 respective lesion marker.

215 To test the efficiency of PARP inhibitor ABT-888, cells were left untreated or pre-
216 treated with 1 µM ABT-888 for increasing time points, followed by DNA damage
217 induction using 800 µM H_2O_2 (Merck) for 10 min. Detection of PAR was achieved after
218 fixation with methanol:acetic acid (3:1) using a monoclonal mouse α-PAR antibody

219 (10H, 1:300 in PBSMT (5 % milk powder, 0.05 % Tween 20, PBS) at 4 °C overnight.
220 Confocal microscopy was performed with a Zeiss LSM 510 Meta as described above.
221 PAR nuclear intensities were analysed using Fiji v1.49u.

222 For superresolution imaging by 3D structured illumination (SI), U2-OS GFP-DEK
223 cells were grown on high precision coverslips (# 1.5). Replication foci were labelled
224 via incubation with 10 µM EdU for 10 min prior fixation. For immunofluorescence
225 detection of PCNA, cells were fixed using 4 % PFA/PBS (10 min) and permeabilized
226 in methanol (5 min, -20 °C). After blocking with 2 % BSA/PBS, cells were incubated
227 with monoclonal mouse α-PCNA primary antibody (PC10, Cell Signaling Technology)
228 diluted 1:2,400 in 10 % NGS/PBS at 4 °C overnight. After washing with 0.05 %
229 Tween/PBS, cells were incubated with goat α-mouse AlexaFluor-568 secondary
230 antibody diluted 1:400 in 10 % NGS/PBS (1 h, RT).After washing with 0.05 %
231 Tween/PBS, cells were fixed again using 2 % PFA/PBS (10 min, RT). EdU was
232 detected using the Klick-it EdU Imaging Kit with azide AlexaFluor-647. Coverslips were
233 mounted on microscopy slides using Vectashield H-1000 (Vector Laboratories).
234 Images were acquired at a DeltaVision OMX Blaze v4 (GE Healthcare) using an
235 Olympus Plan Apochromat 60x/1.42 oil objective. A z-stack of at least 20 slices (0.125
236 µm step size) was acquired per image in SI mode. Reconstruction of SIM images and
237 image registration of the channels was performed using softWoRx v6.5.2 (GE
238 Healthcare). Pseudo-widefield images were generated with Fiji v1.51n and the
239 SIMcheck plugin (v1.0 [47]).

240 Super resolved imaging by stochastic optical reconstruction microscopy (STORM)
241 was carried out on U2-OS GFP-DEK cells cultured in McCoy's 5a modified medium
242 (Thermo Fisher Scientific) supplemented with 10 % fetal bovine serum (FCS;
243 Capricorn Scientific and PAA Laboratories), 100 U/ml penicillin and 100 µg/ml

244 streptomycin (both Thermo Fisher Scientific). For STORM imaging cells were plated
245 on eight-well Lab-Tek coverglass chamber (Nunc), grown under standard conditions
246 and fixed after 24 h. For STORM detection of DEK protein cells were fixed with
247 methanol:ethanol (1:1) at -20 °C for 3 min, washed with PBS following blocking buffer
248 for 2 h at RT (3 % BSA, 0.2% Triton X-100, PBS). After blocking and permeabilization,
249 cells were incubated with primary antibodies diluted in blocking buffer, firstly for 2 h at
250 RT and then overnight at 4 °C. The following primary antibodies were used: polyclonal
251 chicken α-GFP (1:2000; ab13970, Abcam), polyclonal rabbit α-PCNA (1:50;
252 HPA030522, Sigma-Aldrich). After six washing steps with blocking buffer for 5 min
253 each, cells were incubated with secondary antibodies diluted in blocking buffer at RT
254 for 1 h. Specific antibodies were used, namely: donkey α-chicken
255 AlexaFluor405/AlexaFluor647 (1:50; IgG (703-005-155, Jackson ImmunoResearch)
256 coupled to reporter and activator dyes – AlexaFluor405 #A30000, Invitrogen and
257 AlexaFluor647 #A2006), and goat α-rabbit CF568 (1:1000; SAB4600084, Sigma-
258 Aldrich).
259 Single-molecule localisation was performed using a Nikon N-STORM super-resolution
260 microscope equipped with a 100x/1.40 oil-immersion objective lens and coupled to an
261 Andor iXon DU-897E-CS0BV EMCCD camera (image pixel size 160 nm) with 30ms
262 exposure time. To maintain the z-position a Nikon “perfect focus system” was used.
263 The set-up included a 405 nm laser for activation (Coherent CUBE 405 nm; 100 mW)
264 and a 647 nm readout laser (MPBC’s CW Visible Fiber Laser). Imaging was performed
265 using TIRF illumination. 30.000 frames at 25 Hz frame rate were acquired. For
266 widefield imaging together with STORM, a 561 nm laser (Coherent Sapphire OPSL
267 561 nm; 100 mW) was used. Dichroic mirrors and band-pass filters allowed for
268 selection of emitted signals (ZET405/488/561/647, Chroma). For super-resolution

269 measurements, STORM imaging buffer was used (prepared following Nikon's STORM
270 Protocol-Sample Preparation) containing GLOX solution as oxygen scavenging
271 system (40 mg/ml Catalase, Sigma; 0.5 mg/ml glucose oxidase; 10 % glucose in PBS)
272 and MEA 10 mM (Cysteamine MEA, Sigma-Aldrich, #30070-50G, in 360 mM Tris-HCl).
273 Single molecule localization and super-resolution image reconstruction were
274 performed using NIKON software (NIS elements) and a custom software (Insight3,
275 custom software developed by B. Huang, University of California). Molecules are
276 identified and x-y located by Gaussian fitting. The final image is reconstructed, after
277 drift correction, by plotting each identified molecule as a Gaussian spot with a width
278 corresponding to the achieved localization precision (9nm).
279

280 Site-directed mutagenesis

281 Nucleobase mutations of the DEK primary sequence were introduced via a modified
282 Quick ChangeTM site-directed mutagenesis protocol [48]. To generate the DEK-GFP
283 template for the mutagenesis PCR, the DEK WT sequence was inserted into an eGFP
284 reporter plasmid (peGFP-N1, Addgene 6085-1). PAR-binding domain 2 (bases 583 -
285 663) and the DEK shRNA target site (bases 1000 – 1020) were mutated using
286 overlapping primer pairs containing the desired base changes. For the PAR-binding
287 domain a total of 9 codons were mutated in four rounds of mutagenesis (primers
288 PBD2-Part1-4, see also Fig 7 B). For the shRNA target site a total of 8 nucleobases
289 were mutated in two rounds (primers shDEK-Part1-2), resulting in silent mutations and
290 diminished binding of the DEK shRNA. Primer sequences are listed in S1 Table.
291

292 **Expression and purification of recombinant GST-tagged proteins**
293 **from *E. coli***

294 The mutated DEK sequence (DEK PBD2-Mut2) was inserted into a GST expression
295 plasmid. LB_{amp} medium was inoculated with *E.coli* BL21(DE3) pGEX 4T-1 harbouring
296 plasmids encoding GST only, GST-DEK WT, or GST-DEK PBD2-Mut2. Protein
297 expression was induced using 0.5 mM IPTG (Merck) for 1.5 h. Bacteria were
298 harvested via centrifugation (1,600 x g, 15 min, 4 °C), the pellet was resuspended in
299 resuspension buffer (20 mM Tris-HCl pH 8, 1 M NaCl, 0.5 mM EDTA, 1 mM DTT) and
300 shock frozen in liquid nitrogen. Cells were sonicated on ice, 0.5 % NP-40 (Merck) was
301 added and the lysate was centrifuged (18,000 x g, 30 min, 4 °C). The supernatant was
302 incubated with 200 µl Glutathion-Sepharose 4B-beads (GE Healthcare) equilibrated in
303 wash buffer I (20 mM Tris-HCl pH 8, 500 mM NaCl, 0.5 mM EDTA, 1 mM DTT, 0.1 %
304 NP-40) for 2 hours at 4 °C. Beads were washed with wash buffers of decreasing NaCl
305 concentrations (500, 300 and 20 mM NaCl). For elution of GST-tagged DEK, beads
306 were incubated with 200 µl of elution buffer (200 mM Tris-HCl pH 8, 20 mM NaCl, 40
307 mM reduced glutathione, 10 % glycerol) for one hour at 4 °C. The GST-tagged protein
308 containing supernatant was shock frozen in liquid nitrogen and stored at -80 °C.
309 Protein concentrations were determined using the BCA Protein Assay Kit (Thermo
310 Fisher Scientific) according to manufacturer´s instructions.

311

312 **Electrophoretic Mobility Shift Assay (EMSA)**

313 Purified recombinant proteins (GST-DEK WT and GST-DEK PBD2-Mut2) were
314 dialyzed in nE100 buffer (20 mM Hepes-KOH pH 7.6, 100 mM NaCl, 10 mM $NaHSO_3$,
315 1 mM EDTA, supplemented with 1 µg/ml BSA) using Millipore filters (VSWP 0.025 µm;

316 Merck) for 90 min at 4 °C. 175 ng of plasmid DNA were incubated with increasing
317 amounts of recombinant DEK in a total volume of 30 µl nE100 buffer for one hour at
318 37 °C. Samples were subjected to electrophoresis on a 0.6 % agarose gel in TBE
319 buffer (50 mM Tris base, 80 mM boric acid, 1 mM EDTA, pH 8). DNA-protein
320 complexes were visualized with 0.5 µg/ml ethidium bromide solution using a
321 fluorescence imager.
322

323 ## *In-vitro* synthesis of PAR

324 PAR was synthesized and purified according to Fahrer et al. [49]. Briefly, 50 µg/ml
325 'activator' oligonucleotide GGAATTCC and 60 µg/ml of both recombinant Histone H1
326 und H2A were diluted in buffer containing 100 mM Tris-HCl pH 7.8, 10 mM $MgCl_2$ and
327 1 mM DTT. To start the reaction, 1 mM NAD^+ (Merck) and 150 nM recombinant PARP1
328 were supplemented. PAR synthesis was stopped after 15 min by adding ice-cold
329 trichloroacetic acid (TCA) to a final concentration of 10 %. PAR was detached from
330 histones and PARP1 itself using 0.5 M KOH/50 mM EDTA. After neutralization, DNA
331 and proteins were digested using 110 µg/ml DNase and 220 µg/ml proteinase K (both
332 Merck), respectively. PAR was purified by phenol-chloroform-isoamylalcohol
333 extraction and ethanol precipitation. The concentration of the purified polymer was
334 determined via absorbance at 258 nm.
335

336 ## PAR overlay assay

337 60 pmol of custom synthesized PAR-binding domain peptides (for sequences see Fig
338 7 B and S 5 A Fig; biomers.net) or 25 pmol of recombinant GST-tagged proteins were
339 transferred onto a nitrocellulose membrane using a slot blotting apparatus. The

340 membrane was allowed to air-dry and incubated overnight in 5 pmol PAR/TBST (100
341 mM Tris-HCl, 150 mM NaCl, 0.5 % Tween 20) at 4 °C. Blots were blocked in 5 % milk
342 powder/TBST and membrane-bound PAR was detected using monoclonal mouse α-
343 PAR antibody (1:300; 10H). After washing, the membrane was incubated with
344 secondary antibody goat α-mouse Ig/HRP (1:2,000; Agilent). PAR was detected using
345 a chemiluminescence imager. To verify that equal amounts of proteins or peptides
346 were blotted onto membranes, the same protein solutions as used for the PAR overlay
347 were slot blotted onto a nitrocellulose membrane and allowed to air-dry. Samples were
348 fixed in 7 % acetic acid/10 % methanol for 15 min at RT. After fixation, proteins or
349 peptides were stained using Sypro Ruby Protein Blot Stain (Thermo Fisher Scientific)
350 for 15 min and visualized using a Gel Doc XR system (Bio-Rad).
351

352 ## Statistical analysis

353 Statistical tests were performed using GraphPad Prism 5.02 and applied as indicated
354 in the figure legends. $^{*}p \leq 0.05$, $^{**}p \leq 0.01$, $^{***}p \leq 0.001$.
355

356 # RESULTS

357 ## The effect of short term PARP1 inhibition on mildly
358 challenged replication forks is reverted in DEK knockdown
359 cells

360 To investigate whether PARylation regulates the impact of DEK on the replication
361 stress response, we set out from our previous observation that downregulation of DEK
362 expression aggravates replication fork slowing induced by low concentrations of CPT.
363 Inhibition of topoisomerase1 by CPT stabilizes Topo1-cleavable complexes (Top1ccs),
364 thus causing torsional stress ahead of the replication fork. As a result, fork progression
365 is impaired, eventually leading to replisome disassembly and DNA strand breaks. At
366 very low doses (25 nM), CPT was shown to slow down, but not arrest, fork progression
367 and trigger fork reversal in a PARP1/2-dependent manner [10, 11].

368 Firstly, we examined the effect of DEK and PARP1/2 activity on CPT-induced
369 replication fork progression using DNA fiber assays (Fig 1). Cells bearing a stable,
370 lentiviral mediated knockdown of DEK expression (shDEK cells) and the respective
371 control cells [43] were treated with 25 nM CPT in the presence and absence of ABT-
372 888. Both drugs were added simultaneously with the IdU-containing medium (Fig 1 A).
373 In line with our previous results, knockdown of DEK expression slowed down
374 replication fork progression *per se* as indicated by a highly significant reduction of the
375 IdU tract lengths in untreated shDEK cells as compared to controls (Fig 1 C and [43]).
376 Inhibition of PARP1/2 activity with ABT-888 had no significant effect on replication fork
377 speed in both control and shDEK cells, measured as the ratio of the IdU-labelled tracts
378 (green) vs the CldU-labelled tracts (red) (Fig 1 D, compare boxes 1 and 2). Notably,

379 in all our PARP1/2 inhibition experiments, we took care of minimizing DNA damage
380 due to trapping of the enzyme on DNA [7]. Therefore, we used ABT-888 as an inhibitor
381 with reportedly low trapping activity and limited the exposure to the duration of the IdU-
382 pulse. PARP1/2 activity is effectively inhibited under these conditions (S1 A, B Fig) but
383 does not trigger a DNA damage response, as indicated by the absence of 53BP1 foci
384 formation (S1 C, D Fig; see also [50, 51]).
385

386 **Fig 1. Combined inactivation of DEK and PARP1/2 prevents fork slowing by**
387 **low doses of CPT and HU**

388 (A) Scheme of the DNA fiber assay. U2-OS control and shDEK cells were pulse-
389 labelled with CldU for 20 min, followed by incubation with IdU for 20 min in the
390 presence or absence of replication stress inducers (25 nM CPT or 10 µm HU) and 1
391 µM ABT-888. (B) Representative microscopic images of DNA fibers after spreading.
392 Thymidine analogues were visualized via indirect immunofluorescence. CldU-labelled
393 tracts were visualized in the red channel, IdU-labelled tracts in the green channel.
394 Scale bar: 5 µm. (C-D) Quantification of CldU and IdU tract lengths of at least 250
395 fibers per experimental condition. The experiment was performed in triplicates. The
396 bands inside the boxes display the median, whiskers indicate the 5th to 95th percentile
397 and black dots mark outliers. t-test: ns: not significant, *** $p \leq 0.001$. ABT-888 treated
398 cells: hatched bars. (C) Lengths of IdU-labelled tracts. (D) IdU/CldU tract length ratios.
399

400 Treatment with low doses of CPT reduced fork progression, as expected, in control
401 cells and, to a greater extent, in shDEK cells (Fig 1 D, compare boxes 3 and 9). When
402 exposure to CPT occurred in the presence of ABT-888, the two cells lines, however,
403 showed opposite responses: in control cells, the replication fork was further retarded

404 as compared to treatment with CPT only, while in shDEK cells, fork speed recovered
405 to the basal level measured in the absence of any perturbation (Fig 1 D, compare
406 boxes 4 and 10). Further, in the presence of CPT, the extent of fork slowing obtained
407 by inhibiting PARP1/2 in control cells equalled that resulting from downregulation of
408 DEK expression (Fig 1 D, compare boxes 4 and 9), which is suggestive of DEK and
409 PARP1/2 acting in the same regulatory pathway.

410 We sought to validate these observations in a different replication stress model and
411 performed fiber assays using low doses of hydroxyurea (HU). At 10 μm, HU slows
412 down but does not stall the replication fork as observed at higher concentrations (e.g.
413 2mM, compare Fig 1 D with S2 Fig). Again, additional PARP1/2 inhibition positively
414 impacted on fork progression in shDEK cells, but not in control cells (Fig 1 D, compare
415 boxes 6 and 12). Interestingly, this modulatory effect was detectable only under mild
416 replication stress conditions. At a concentration of HU of 2 mM, combined exposure
417 to ABT-888 did not alter fork speed, although in general, replication forks of shDEK
418 cells were significantly more sensitive to HU-mediated stalling than those of control
419 cells (S2 Fig). Finally, the fork acceleration observed in mildly stressed, PARylation
420 inhibited shDEK cells was not sufficient to compensate for the fork impairment caused
421 by DEK downregulation itself, because the IdU tract length in stressed and PARP1/2-
422 inhibited shDEK cells remained shorter than in control untreated cells (Fig 1 C).

423 As replication stress is a source of DNA damage, we evaluated whether DEK
424 downregulation would also affect the formation of DNA strand breaks caused by
425 exposure to replication inhibitors and ABT-888. We assessed replication-associated
426 DSBs by counting γH2AX/53BP1 double-positive foci in EdU-positive S-phase shDEK
427 and control cells. In the case of CPT, DNA strand breaks are known to arise when the
428 transcription and/or replication machineries collide with unrepaired Top1ccs. At 25 nM

429 CPT, the overall response was very moderate as expected at this subtoxic dose [11].
430 Only 7 foci were observed on average in control cells (Fig 2 A, B). This low number
431 was nevertheless significantly higher in shDEK cells, in line with our previous data
432 showing that DEK downregulation sensitizes cells to CPT treatment [20]. The
433 combination of CPT and PARP1/2 inhibition led to an increase in DSBs in control cells,
434 while shDEK cells showed a significant reduction, resembling the pattern observed
435 with our fiber assays. These data suggest that the restoration of fork speed observed
436 in CPT-treated, DEK-depleted cells when PARP1/2 is inhibited is not a manifestation
437 of fork run off. Most likely, this effect reflects the ability of shDEK cells to either
438 withstand the action of CPT or better cope with its consequences, if PARP1/2 activity
439 is blocked. Unfortunately, this assumption could not be confirmed in the HU-model of
440 replication stress, since exposure to 10 μM HU did not result in a measurable DNA
441 damage response in our experimental setting (Fig 2 A, B).
442

443 **Fig 2. Combined inactivation of DEK and PARP1/2 counteracts DNA damage**
444 **induced by low doses of CPT**

445 U2-OS control and shDEK cells were pulse-labelled with EdU, then either left
446 untreated or treated with replication stress inducers (25 nM CPT or 10 μm HU) for one
447 hour, in the presence or absence of 1 μM ABT-888. 53BP1 (red) and γH2AX (green)
448 foci formation was visualized via indirect immunofluorescence analysis, EdU (magenta)
449 using click chemistry. DNA was counterstained with Hoechst 33342 (cyan). (A)
450 Representative confocal images. Scale bar: 5 μm. (B) Quantification of 53BP1/γH2AX
451 colocalization in S-phase cells. Foci were counted and colocalization determined using
452 the foci counter of the BIC macro tool box. At least 118 cells per experimental condition
453 were evaluated. The experiment was performed in triplicates. The bands inside the

454 boxes display the median, whiskers indicate the 5th to 95th percentile and outliers are
455 omitted for clarity. t-test: *** p≤0.001.
456
457 Altogether, these data show that the outcome of acute PARP1/2 inhibition on
458 challenged replication forks is dependent on DEK expression levels and suggest the
459 existence of a regulatory network involving DEK and PARP1/2 that modulates fork
460 speed. This interaction is only detectable under mild stress levels, when the fork is still
461 processive.
462

463 DEK is not part of the replisome but binds to newly 464 replicated DNA as it matures to chromatin

465 The marked effects of DEK expression on fork progression let us explore whether DEK
466 directly associates to replication forks. To this end, we performed iPOND (isolation of
467 proteins on nascent DNA) assays [44]. Firstly, we treated HeLa S3 cells with EdU for
468 increasing time periods (2.5 min – 30 min) to label newly synthesized DNA and
469 subsequently monitored the occurrence of DEK in the pool of enriched proteins by
470 Western Blot (Fig 3 A-C). We used PCNA to monitor the active replisome while histone
471 H3 served as marker for maturing chromatin. PCNA was detected at early time points
472 (5 min and 10 min) representing nascent DNA. DEK lagged behind and appeared after
473 an EdU pulse of 15 min duration, concomitantly with H3. We corroborated this result
474 with an iPOND pulse-chase experiment, in which we sought to observe the dynamics
475 of DEK binding to nascent chromatin (Fig 3 D-F). EdU was applied for 10 min to pulse-
476 label nascent DNA and then replaced with thymidine for increasing time periods before
477 the isolation of proteins crosslinked to DNA. Proteins binding directly and exclusively

478 at the replication fork diminish in the enriched protein fraction as the EdU labelled DNA
479 stretch moves away from the fork, as exemplified by PCNA. In line with the pulse-only
480 experiment, DEK was found to bind at later time points, with relative Western Blot
481 signal intensities increasing to significance at 15 to 30 min after thymidine addition.
482 Here too, DEK behaved similarly to histone H3. From these experiments we conclude
483 that DEK is not a component of the active replisome but rather binds to DNA as it
484 assembles into mature chromatin.
485

486 **Fig 3. DEK is not a component of the replisome**

487 (A-C) HeLa S3 cells were pulse-labelled with EdU for 2.5 – 30 min and biotin-azide
488 was covalently attached via click chemistry. After cell lysis, EdU-biotin containing DNA
489 fragments were precipitated using streptavidin-coupled magnetic beads. Bound
490 proteins (capture) were identified by Western blot analysis. (A) Scheme of iPOND
491 pulse experiment. (B) Representative Western blots of input and capture samples
492 using antibodies specific for DEK, PCNA and histone H3. (C) Densitometric analysis.
493 The fold change of captured protein is displayed relative to the value of the 30 min
494 time point. Band intensities of capture samples were normalized to the respective input
495 smaples. Shown are mean values from five independent experiments. One-sided error
496 bars represent the S.D. 2way ANOVA with Bonferroni posttest: * $p \leq 0.05$, ** $p \leq 0.01$,
497 *** $p \leq 0.001$.

498 (D-F) HeLa S3 cells were pulse-labelled with EdU for 10 min, followed by a chase into
499 thymidine containing medium for 0 – 30 min. iPOND was performed as in (A-C). (D)
500 Scheme of iPOND chase experiment. (E) Representative Western blots of input and
501 capture samples using antibodies specific for DEK, PCNA and histone H3. (F)
502 Densitometric analysis. The fold change of captured protein is displayed relative to the

503 value of the 0 min time point. Band intensities were normalized as in (C). Shown are
504 mean values from five independent experiments, one-sided error bars represent the
505 S.D. 2way ANOVA with Bonferroni posttest: * p≤0.05, ** p≤0.01, *** p≤0.001.
506
507 To complement this biochemical approach we studied the localization of DEK in
508 replicating cells by superresolution microscopy (Fig 4). To this purpose, we took
509 advantage of a U2-OS knock-in cell line expressing GFP-DEK from its endogenous
510 promoter (Vogel et al, in preparation). Firstly, we employed structured illumination
511 microscopy [52] and combined EdU labelling of nascent DNA with immunolabeling of
512 PCNA. The images showed that DEK does not colocalize with sites of active
513 replication (Fig 4 A). This finding was corroborated by stochastic optical reconstruction
514 microscopy (STORM, Fig 4 B) [53]. This approach offers a key chance to investigate
515 the distribution of nuclear proteins at the nanoscale level [54]. Also at this higher
516 resolution, DEK is not found colocalizing with PCNA. Presently, we cannot exclude
517 that the localization of DEK with respect to active replication foci may vary during S-
518 phase progression, thus accounting for a partial enrichment of DEK in late chromatin
519 fractions in iPOND experiments. Altogether, based on these data, we can exclude that
520 DEK is part of the replisome making it very unlikely that its function in promoting
521 replication fork progression occurs via a direct interaction.
522
523 **Fig 4. DEK does not colocalize with replication foci in superresolution images**
524 (A) 3D-SIM superresolution microscopy images of DEK, EdU and PCNA distribution
525 in early/mid S-phase. U2-OS GFP-DEK cells were treated with EdU for 10 min to label
526 nascent DNA via click chemistry, and PCNA was visualized via indirect
527 immunofluorescence. Shown is a single z-slice from the super-resolved image stack

528 with two magnified insets. Red: GFP-DEK, green: PCNA (green), magenta: EdU.
529 Upper left corner: Pseudo-widefield representation of the same nucleus by
530 superimposition of all z-slices. (B) STORM superresolution microscopy images of DEK
531 and PCNA distribution in early S-phase. DEK (red) and PCNA (green) were visualized
532 via indirect immunofluorescence in U2-OS GFP-DEK cells with Alexa405/Alexa647
533 photoswitchable dye pairs respectively CF568. Shown is a single z-slice with two
534 magnified insets. Top left corner: Widefield image of the same nucleus.
535

536 Fork restart impairment observed under PARP1/2 inhibition 537 depends on DEK expression

538 As we had observed that the effect of PARP1/2 inhibition on mildly impaired replication
539 forks depended on DEK expression, we asked whether DEK levels would also impinge
540 on the recovery of replication forks after stalling. PARP1/2 was shown to protect
541 replication forks stalled by HU treatment and promote their effective restart [8, 9, 55],
542 providing a suitable experimental paradigm to evaluate the effect of DEK
543 downregulation.

544 We performed DNA fiber assays in shDEK and control cells in which forks were
545 completely blocked using a prolonged exposure to a high dose of HU (4 mM for 4 h,
546 see also S3 Fig), followed by removal of HU and release in fresh medium in the
547 presence and absence of ABT-888 (Fig 5 A). Downregulation of DEK alone had no
548 effect on the resumption of DNA synthesis after removal of HU, with about 80% of
549 forks restarting in both control and shDEK cells. In the former, PARP1/2 inhibition led
550 to a marked decrease of fork restart efficiency to about 60%, in line with published
551 results [8]. In contrast, shDEK cells were completely protected from restart impairment,

552 displaying a slightly higher number of restarting forks as compared to control cells not
553 exposed to ABT-888 (Fig 5 C). These data reflect the same phenotype of DEK
554 downregulation counteracting PARP1/2 inhibition as observed in the context of fork
555 slowing by CPT, and underscore its functional relevance.
556
557 **Fig 5. DEK depletion counteracts fork restart impairment due to PARP1/2**
558 **inhibition**
559 (A-C) U2-OS control and shDEK cells were pulse-labelled with CldU for 20 min,
560 followed by incubation with 4 mM HU for four hours to arrest replication forks. Forks
561 were released in fresh IdU-containing medium in the presence or absence of 1 μM
562 ABT-888. (A) Scheme of the fork restart experiment. (B) Representative confocal
563 images for each experimental condition. CldU-labelled tracts were visualized in the
564 red channel, IdU-labelled tracts in the green channel. Scale bar: 5 μm. (C)
565 Quantification of results. The mean percentage of restarting forks from three
566 independent experiments is shown. At least 300 fiber tracts were scored per
567 experimental condition. Error bars represent the S.E.M. t-test: ns: not significant, *
568 $p \leq 0.05$, ** $p \leq 0.01$. ABT-888 treated cells: hatched bars.
569
570 Fork impairment and stalling by HU treatment has been shown previously to elicit the
571 robust formation of RPA-positive foci [56], reflecting RPA binding to single stranded
572 DNA (ssDNA) which is extensively generated when polymerase and helicase activity
573 are uncoupled. RPA protects this ssDNA from nucleolytic attack and serves multiple
574 important functions in the repair and restart of damaged forks [57, 58]. To further
575 investigate the effect of DEK expression on impaired replication forks we determined
576 the formation of RPA-positive foci under conditions of replication stress combined with

577 PARylation inhibition (Fig 6). We applied 2 mM HU for 80 min, as this dose and time
578 of exposure was shown to elicit a maximal HU response in U2-OS cells [56], and
579 measured RPA foci in EdU positive cells (see also S4 Fig for the quantification method).
580 As observed for fork slowing and DSB formation, shDEK cells showed a significantly
581 increased RPA response as compared to control cells. In the latter, additional
582 PARP1/2 inhibition reduced the formation of RPA foci with respect to HU treatment
583 only. This finding is in line with data from Bryant et al. [8] who reported reduced RPA
584 foci in PARP-inhibited cells. Again, shDEK cells reacted differently, displaying a small,
585 but significant increase in RPA-positive cells when exposed to HU in combination with
586 ABT-888 (Fig 6 B). These data suggest that DEK plays a role in limiting the formation
587 of long ssDNA stretches upon stalling or collapse of replication forks, and that its
588 downregulation compensates for the previously described requirement for PARP1/2
589 activity for RPA binding at a subpopulation of stalled forks. These results further
590 corroborate the existence of a reciprocal functional link between DEK and PARP1/2 in
591 the response to replication stress.
592

593 **Fig 6. DEK counteracts the effect of ABT-888 on RPA foci formation under HU**
594 **treatment**

595 (A-B) U2-OS control and shDEK cells were pulse-labelled with EdU, then either left
596 untreated or treated with 2 mM HU for 80 min in presence or absence of 1 μM ABT-
597 888. RPA foci (green) were visualized via indirect immunofluorescence, EdU (magenta)
598 using click chemistry. DNA was counterstained with Hoechst 33342 (cyan). (A)
599 Representative confocal images for each experimental condition. Scale bar: 5 μm. (B)
600 Percentage of RPA positive S-phase cells as determined using the automated foci
601 counter of the BIC macro tool box (see also S4 Fig). Mean values from three

602 independent experiments are shown. At least 97 cells were scored per experimental
603 condition. Error bars represent the S.E.M. t-test: *p≤0.05, **p≤0.01.
604

605 A DEK mutant with impaired PAR-interaction ability 606 counteracts the effect of DEK downregulation on the 607 response to replication fork stalling

608 In our previous work we described that DEK is modified by PAR covalently and non-
609 covalently [18, 20, 49]. Interestingly, DEK shows a remarkably high affinity for long
610 PAR chains exceeding that of histone H1. Therefore, we hypothesized that
611 noncovalent DEK-PAR interaction would be important to mediate the effect of DEK on
612 challenged replication forks. To verify this hypothesis, we sought to obtain a PAR-
613 binding deficient mutant of DEK. We performed a systematic mutational study of the
614 three previously described PAR-binding domains (PBDs) in the DEK primary
615 sequence (PBD1: aa 158-181, PBD2: aa 195-222; PBD3: aa 329-352; Fig 7 A and S1
616 Table). Previous *in vitro* studies showed that they have different affinities for purified
617 PAR. The strongest PAR binding domain in the DEK primary sequence is PBD2 at
618 amino acid positions 195-222, partially overlapping with the SAP-box of DEK, which
619 is its major DNA-binding domain [18]. Mutant peptides corresponding to the three
620 PAR-binding domains of DEK were subjected to PAR-overlay assays to assess the
621 effect of single and multiple amino acid exchanges on PAR binding *in vitro* (Fig 7 B,
622 C; S5 Fig). We were able to identify mutations within the high-affinity PBD2 peptide
623 which completely abrogated non-covalent PAR interaction (Fig 7 B, C, Mut1-3).
624 Moreover, when peptides corresponding to the three PBDs were incubated
625 simultaneously with purified PAR in the same slot blot, only peptide 195-222 gave rise

626 to PAR-specific signals, suggesting that this domain is the predominant PAR-acceptor
627 in DEK, outcompeting the weaker PBDs (data not shown). We then generated purified
628 recombinant DEK carrying a mutated PBD2 (Mut2) and tested the effect of the
629 identified mutations in the context of the full-length protein (Fig 7 D). By densitometric
630 analysis we observed a reduction in PAR-binding affinity of about 50% as compared
631 to the corresponding wildtype DEK sequence, confirming the data obtained with the
632 isolated peptides. The overall DNA binding ability of the PBD2-Mut2 mutant was only
633 slightly reduced as compared to the wildtype DEK. A band shift in EMSA assays
634 became detectable at a molar ratio of DEK:DNA of 112 instead of 84. At higher molar
635 ratios the binding behaviour of the two proteins was undistinguishable (Fig 7 E).
636

637 **Fig 7. Non-covalent interaction of DEK with PAR is important for RPA foci**
638 **formation upon HU treatment**

639 (A) Schematic of the DEK protein with PAR-binding domains and DNA interaction sites.
640 (B) Mutational analysis of PBD2 using recombinant peptides. Basic (green) and/or
641 hydrophobic (blue) amino acids were exchanged for alanine (red) as indicated. (C)
642 Peptides were analysed in a PAR overlay assay to assess PAR-binding. PAR was
643 detected by chemiluminescence using a specific antibody (α-PAR-10H). Equal
644 membrane loading of peptides was verified using Sypro Ruby. One representative blot
645 is shown. The experiment was performed in triplicate with similar results. (D)
646 Recombinant full-length GST-DEK WT and GST-DEK PBD2-Mut2 were purified from
647 *E.coli* and analysed using PAR-overlay assays. One representative blot out of two
648 replicates is shown. (E) Analysis of the DNA binding ability of GST-DEK WT and GST-
649 DEK PBD2-Mut2 via EMSA. Recombinant proteins were incubated with plasmid DNA
650 in increasing molar ratios. DEK/DNA complexes were separated on agarose gels and

651 visualized using ethidium bromide. One representative gel out of two replicates is
652 shown. (F) Analysis of RPA foci formation. U2-OS shDEK cells were transfected with
653 plasmids encoding GFP fused to either WT-DEK or DEK PBD2-Mut2. GFP-positive,
654 low-level expressing cells were isolated by FACS. U2-OS control and shDEK cells
655 expressing GFP-DEK fusion proteins were treated with 2 mM HU for 80 min. RPA foci
656 formation was analysed by immunofluorescence as described in Fig 6, S-phase cells
657 were identified by EdU labelling. The percentage of RPA positive S-phase cells was
658 determined using the automated foci counter of the BIC macro tool box. The mean
659 values from three independent experiments are shown. At least 100 cells were scored
660 per experimental condition. Error bars represent the S.E.M. t-test: ns: not significant,
661 * $p \leq 0.05$.
662
663 We then used the PDB2-Mut2 mutant to analyse the influence of PARylation of DEK
664 on the formation of RPA foci upon fork stalling. Wildtype or PBD2-Mut2-DEK fused to
665 GFP were expressed in shDEK and control cells and the number of RPA-positive cells
666 after HU treatment was determined as above. Both GFP fusion proteins were
667 expressed at comparable levels as verified by Western blot (S6 Fig).
668 Treatment with 2 mM HU robustly triggered RPA foci formation, to a higher level in
669 shDEK cells as compared to controls, as already observed (Fig 7 F). Re-expression
670 of WT DEK abrogated this effect confirming its specificity and reducing the number of
671 RPA-positive cells to a level below that of HU-treated control cells. Importantly, the
672 DEK mutant with reduced PAR-binding ability was much less effective in counteracting
673 RPA-foci formation. We conclude from this result that the increase in HU-induced RPA
674 foci mediated by DEK requires its non-covalent interaction with PAR. We cannot rule
675 out, however, that other mechanisms and/or PAR-binding domains of DEK may be

676 involved too, because the PBD2-Mut2 did not fully restore the level of RPA foci
677 obtained in shDEK cells after HU treatment (Fig 7 F). Taken together, these data
678 strongly suggest that the non-covalent interaction with PAR plays a major role in
679 regulating how DEK affects the response to replication stress providing a first
680 mechanistic insight in the complex molecular interplay of PARP1/2 and DEK.
681

682 # DISCUSSION

683 In this study we have explored a potential functional relationship between DEK and
684 PARP1/2 in the context of DNA replication stress. For both proteins, there is consistent
685 evidence for their involvement in the response to impaired DNA replication. Both DEK
686 and PARP1/2 preferentially bind to unconventional non-B DNA structures like
687 cruciform and G4 DNA [36, 59-61]. These structures are difficult to replicate and
688 particularly abundant in heterochromatin. Both DEK and PARP1/2 are found enriched
689 in chromatin of S-phase cells [62-65] and have been associated with the formation
690 and maintenance of heterochromatin [39, 66]. DEK was shown to modulate the
691 efficiency of DNA replication *in vitro* [42], and, more recently, we showed that normal
692 DEK levels are necessary to sustain replication fork progression and to prevent fork
693 rearrangements in cells undergoing replication stress [43]. DEK is a target for covalent
694 modification by and non-covalent interaction with PAR. Covalent PARylation was
695 reported to occur at glutamic acid 136 [67] and 207 [68], arginine 208 [68] and, most
696 recently, at serine 279 [69]. Based on sequence alignment, DEK was further proposed
697 to harbour three non-covalent PAR-binding domains [18], of which the central one (aa
698 position 195-222) shows the strongest binding affinity and mediates about 50% of the
699 PAR-binding activity of the protein *in vitro* (this study and [70]).

700 Impaired replication forks can activate PARP1/2 and PAR has been involved in the
701 regulation of different types of fork processing and rearrangements. Thus, PARP1/2
702 can protect replication forks from extensive Mre11-dependent resection after HU
703 treatment [8, 9], or from untimely resolution of RecQ-mediated reversal in cells treated
704 with low doses of CPT [11]. Massive accumulation PAR, on the other hand, has
705 adverse consequences. HU-induced prolonged fork stalling in cells with
706 downregulated PAR glycohydrolase (PARG) leads to fork collapse and DSB formation
707 [71]. The molecular events orchestrated by PARP1/2 activation during DNA replication
708 therefore seem to depend, in a yet poorly understood fashion, on the type and extent
709 of the replication problem, which in turn determine the amount and possibly also the
710 structure of the polymer formed. Consequently, inhibiting PARylation during DNA
711 replication may have different outcomes, depending not only on the dose and the
712 duration of the inhibitor treatment but also on the status of the replication machinery.
713 As shown here, short term inhibition of PARP1/2 using ABT-888 aggravates fork
714 retardation and DNA damage induced by mild replication stress, while long term
715 exposure to AZD-2281 was shown to accelerate fork speed both in the presence and
716 in the absence of DNA replication inhibitors [10, 72]. Our data on fork progression in
717 shDEK cells suggest that challenged replication forks can switch between two
718 opposing responses to PARP1/2 inhibition depending on the level of DEK expression.
719 Interestingly, the restoration of fork speed observed in CPT-treated, PARP-inhibited
720 shDEK cells was accompanied by a reduction in the level of replication-associated
721 DSBs. This is in agreement with the finding that fork acceleration activates the DNA
722 damage response only if fork speed exceeds a critical threshold [72], and poses an
723 argument against replication fork runoff occurring in CPT-treated shDEK cells upon
724 treatment with ABT-888. The behaviour of forks stalled by high doses of HU followed

725 a similar pattern with respect to PARP-inhibition and DEK downregulation as CPT-
726 induced fork slowing, being most efficiently restored in PARP-inhibited shDEK cells,
727 which is suggestive of a common mechanism.
728 How DEK affects the sensitivity of replication forks towards PARP inhibition, is a matter
729 of speculation so far. Based on our iPOND and superresolution microscopy data it
730 seems unlikely that DEK acts directly at the fork, since we did not find it associated to
731 nascent DNA before the stage of nucleosome formation. Rather, the data presented
732 here lend credit to the hypothesis that DEK is part of a DNA replication regulatory
733 circuitry orchestrated by PAR that affects response to acute PARPi treatment.
734 Recently, a fork speed regulatory network has been proposed which controls
735 replication fork progression via PARylation and the p53-p21 axis [72]. Both p21 and
736 PAR act as suppressors of fork speed in an interdependent manner, as PARP1
737 additionally represses p21 expression. Intriguingly, downregulation of DEK expression
738 was shown to result in p53 stabilization and increased p21 levels [32], alterations
739 which may indirectly affect the response of fork speed to PARP1/2 inhibitors. Since a
740 PAR-binding defective mutant of DEK partially rescued fork restart impairment by
741 PARP inhibition we cannot exclude that DEK exerts its influence also by directly
742 participating in the PARylation mediated sensing of replication problems. Altogether,
743 this study pinpoints DEK as an important mediator of the PARP1/2-dependent
744 response of replicating cells to fork impairment, a previously unrecognized function of
745 DEK which has implications for tumor therapy and warrants further investigation.

ACKNOWLEDGEMENTS

We thank Eva Gwosch for providing U2-OS GFP-DEK cells, and Aswin Mangerich, Martin Stöckl and the whole BIC team for fruitful discussions. Further, we thank Anja Deutzmann for initial input in this study, and the FlowKon core facility at the University of Konstanz for cell sorting.

REFERENCES

1. Palazzo L, Ahel I. PARPs in genome stability and signal transduction: implications for cancer therapy. Biochem Soc Trans. 2018. doi: 10.1042/BST20180418.
2. Bai P. Biology of Poly(ADP-Ribose) Polymerases: The Factotums of Cell Maintenance. Molecular cell. 2015;58(6):947-58. doi: 10.1016/j.molcel.2015.01.034.
3. Miwa M, Sugimura T. Splitting of the ribose-ribose linkage of poly(adenosine diphosphate-robose) by a calf thymus extract. J Biol Chem. 1971;246(20):6362-4.
4. Kurnit KC, Coleman RL, Westin SN. Using PARP Inhibitors in the Treatment of Patients With Ovarian Cancer. Curr Treat Options Oncol. 2018;19(12):1. doi: 10.1007/s11864-018-0572-7.
5. Bryant HE, Schultz N, Thomas HD, Parker KM, Flower D, Lopez E, et al. Specific killing of BRCA2-deficient tumours with inhibitors of poly(ADP-ribose) polymerase. Nature. 2005;434(7035):913-7. doi: 10.1038/nature03443.
6. Farmer H, McCabe N, Lord CJ, Tutt AN, Johnson DA, Richardson TB, et al. Targeting the DNA repair defect in BRCA mutant cells as a therapeutic strategy. Nature. 2005;434(7035):917-21. doi: 10.1038/nature03445.
7. Murai J, Huang S-yN, Das BB, Renaud A, Zhang Y, Doroshow JH, et al. Differential trapping of PARP1 and PARP2 by clinical PARP inhibitors. Cancer research. 2012;72(21):5588-99. doi: 10.1158/0008-5472.CAN-12-2753.
8. Bryant HE, Petermann E, Schultz N, Jemth AS, Loseva O, Issaeva N, et al. PARP is activated at stalled forks to mediate Mre11-dependent replication restart and recombination. EMBO J. 2009;28(17):2601-15. Epub 2009/07/25. doi: emboj2009206
9. Ying S, Hamdy FC, Helleday T. Mre11-dependent degradation of stalled DNA replication forks is prevented by BRCA2 and PARP1. Cancer Res. 2012;72(11):2814-21. Epub 2012/03/27. doi: 10.1158/0008-5472.can-11-3417.
10. Berti M, Ray Chaudhuri A, Thangavel S, Gomathinayagam S, Kenig S, Vujanovic M, et al. Human RECQ1 promotes restart of replication forks reversed by DNA topoisomerase I inhibition. Nature structural & molecular biology. 2013;20(3):347-54. doi: 10.1038/nsmb.2501.
11. Ray Chaudhuri A, Hashimoto Y, Herrador R, Neelsen KJ, Fachinetti D, Bermejo R, et al. Topoisomerase I poisoning results in PARP-mediated replication fork reversal. Nature structural & molecular biology. 2012;19(4):417-23. doi: 10.1038/nsmb.2258.
12. Hanzlikova H, Kalasova I, Demin AA, Pennicott LE, Cihlarova Z, Caldecott KW. The Importance of Poly(ADP-Ribose) Polymerase as a Sensor of Unligated Okazaki Fragments during DNA Replication. Molecular cell. 2018;71(2):319-31 e3. doi: 10.1016/j.molcel.2018.06.004.
13. Waldmann T, Scholten I, Kappes F, Hu HG, Knippers R. The DEK protein-an abundant and ubiquitous constituent of mammalian chromatin. Gene. 2004;343(1):1-9.
14. Kappes F, Damoc C, Knippers R, Przybylski M, Pinna LA, Gruss C. Phosphorylation by protein kinase CK2 changes the DNA binding properties of the human chromatin protein DEK. Mol Cell Biol. 2004;24(13):6011-20. Epub 2004/06/17. doi: 10.1128/MCB.24.13.6011-6020.2004.

798 15. Kappes F, Scholten I, Richter N, Gruss C, Waldmann T. Functional domains of
799 the ubiquitous chromatin protein DEK. Mol Cell Biol. 2004;24(13):6000-10. Epub
800 2004/06/17. doi: 10.1128/MCB.24.13.6000-6010.2004.
801 16. Cleary J, Sitwala KV, Khodadoust MS, Kwok RP, Mor-Vaknin N, Cebrat M, et al.
802 p300/CBP-associated factor drives DEK into interchromatin granule clusters. J Biol
803 Chem. 2005;280(36):31760-7. Epub 2005/07/01. doi: 10.1074/jbc.M500884200.
804 17. Mor-Vaknin N, Kappes F, Dick AE, Legendre M, Damoc C, Teitz-Tennenbaum
805 S, et al. DEK in the synovium of patients with juvenile idiopathic arthritis:
806 characterization of DEK antibodies and posttranslational modification of the DEK
807 autoantigen. Arthritis Rheum. 2011;63(2):556-67. Epub 2011/02/01. doi:
808 10.1002/art.30138.
809 18. Fahrer J, Popp O, Malanga M, Beneke S, Markovitz DM, Ferrando-May E, et al.
810 High-affinity interaction of poly(ADP-ribose) and the human DEK oncoprotein
811 depends upon chain length. Biochemistry. 2010;49(33):7119-30. doi:
812 10.1021/bi1004365.
813 19. Gamble MJ, Fisher RP. SET and PARP1 remove DEK from chromatin to permit
814 access by the transcription machinery. Nature structural & molecular biology.
815 2007;14(6):548-55. Epub 2007/05/29. doi: 10.1038/nsmb1248.
816 20. Kappes F, Fahrer J, Khodadoust MS, Tabbert A, Strasser C, Mor-Vaknin N, et
817 al. DEK is a poly(ADP-ribose) acceptor in apoptosis and mediates resistance to
818 genotoxic stress. Mol Cell Biol. 2008;28(10):3245-57.
819 21. Wise-Draper TM, Allen HV, Thobe MN, Jones EE, Habash KB, Munger K, et al.
820 The human DEK proto-oncogene is a senescence inhibitor and an upregulated
821 target of high-risk human papillomavirus E7. J Virol. 2005;79(22):14309-17.
822 22. Privette Vinnedge LM, McClaine R, Wagh PK, Wikenheiser-Brokamp KA, Waltz
823 SE, Wells SI. The human DEK oncogene stimulates beta-catenin signaling,
824 invasion and mammosphere formation in breast cancer. Oncogene.
825 2011;30(24):2741-52. Epub 2011/02/15. doi: 10.1038/onc.2011.2.
826 23. Hacker KE, Bolland DE, Tan L, Saha AK, Niknafs YS, Markovitz DM, et al. The
827 DEK Oncoprotein Functions in Ovarian Cancer Growth and Survival. Neoplasia.
828 2018;20(12):1209-18. doi: 10.1016/j.neo.2018.10.005.
829 24. Han S, Xuan Y, Liu S, Zhang M, Jin D, Jin R, et al. Clinicopathological
830 significance of DEK overexpression in serous ovarian tumors. Pathol Int.
831 2009;59(7):443-7. doi: 10.1111/j.1440-1827.2009.02392.x.
832 25. Grasemann C, Gratias S, Stephan H, Schuler A, Schramm A, Klein-Hitpass L, et
833 al. Gains and overexpression identify DEK and E2F3 as targets of chromosome 6p
834 gains in retinoblastoma. Oncogene. 2005;24(42):6441-9. Epub 2005/07/12. doi:
835 10.1038/sj.onc.1208792.
836 26. Lin L, Piao J, Gao W, Piao Y, Jin G, Ma Y, et al. DEK over expression as an
837 independent biomarker for poor prognosis in colorectal cancer. BMC Cancer.
838 2013;13:366. Epub 2013/08/02. doi: 10.1186/1471-2407-13-366.
839 27. Datta A, Adelson ME, Mogilevkin Y, Mordechai E, Sidi AA, Trama JP.
840 Oncoprotein DEK as a tissue and urinary biomarker for bladder cancer. BMC
841 Cancer. 2011;11:234-. doi: 10.1186/1471-2407-11-234.
842 28. Kappes F, Khodadoust MS, Yu L, Kim DS, Fullen DR, Markovitz DM, et al. DEK
843 expression in melanocytic lesions. Hum Pathol. 2011;42(7):932-8. Epub
844 2011/02/15. doi: 10.1016/j.humpath.2010.10.022.
845 29. Riveiro-Falkenbach E, Ruano Y, Garcia-Martin RM, Lora D, Cifdaloz M,
846 Acquadro F, et al. DEK oncogene is overexpressed during melanoma progression.

847 Pigment Cell Melanoma Res. 2017;30(2):194-202. Epub 2016/11/29. doi:
848 10.1111/pcmr.12563.
849 30. Smith EA, Krumpelbeck EF, Jegga AG, Prell M, Matrka MM, Kappes F, et al. The
850 nuclear DEK interactome supports multi-functionality. Proteins. 2018;86(1):88-97.
851 doi: 10.1002/prot.25411.
852 31. Saha AK, Kappes F, Mundade A, Deutzmann A, Rosmarin DM, Legendre M, et
853 al. Intercellular trafficking of the nuclear oncoprotein DEK. Proceedings of the
854 National Academy of Sciences of the United States of America. 2013;110(17):6847-
855 52. doi: 10.1073/pnas.1220751110.
856 32. Wise-Draper TM, Allen HV, Jones EE, Habash KB, Matsuo H, Wells SI.
857 Apoptosis inhibition by the human DEK oncoprotein involves interference with p53
858 functions. Mol Cell Biol. 2006;26(20):7506-19.
859 33. Khodadoust MS, Verhaegen M, Kappes F, Riveiro-Falkenbach E, Cigudosa JC,
860 Kim DS, et al. Melanoma proliferation and chemoresistance controlled by the DEK
861 oncogene. Cancer Res. 2009;69(16):6405-13. Epub 2009/08/15.]
862 34. Zhou QC, Deng XF, Yang J, Jiang H, Qiao MX, Liu HH, et al. Oncogene DEK is
863 highly expressed in lung cancerous tissues and positively regulates cell proliferation
864 as well as invasion. Oncol Lett. 2018;15(6):8573-81. doi: 10.3892/ol.2018.8436.
865 35. Waldmann T, Eckerich C, Baack M, Gruss C. The ubiquitous chromatin protein
866 DEK alters the structure of DNA by introducing positive supercoils. J Biol Chem.
867 2002;277(28):24988-94.
868 36. Waldmann T, Baack M, Richter N, Gruss C. Structure-specific binding of the
869 proto-oncogene protein DEK to DNA. Nucleic Acids Res. 2003;31(23):7003-10.
870 37. Privette Vinnedge LM, Kappes F, Nassar N, Wells SI. Stacking the DEK: from
871 chromatin topology to cancer stem cells. Cell cycle. 2013;12(1):51-66. doi:
872 10.4161/cc.23121.
873 38. Soares LM, Zanier K, Mackereth C, Sattler M, Valcarcel J. Intron removal
874 requires proofreading of U2AF/3' splice site recognition by DEK. Science.
875 2006;312(5782):1961-5. Epub 2006/07/01. doi: 10.1126/science.1128659.
876 39. Kappes F, Waldmann T, Mathew V, Yu J, Zhang L, Khodadoust MS, et al. The
877 DEK oncoprotein is a Su(var) that is essential to heterochromatin integrity. Genes
878 & development. 2011;25(7):673-8. Epub 2011/04/05. doi: 10.1101/gad.2036411.
879 40. Kavanaugh GM, Wise-Draper TM, Morreale RJ, Morrison MA, Gole B,
880 Schwemberger S, et al. The human DEK oncogene regulates DNA damage
881 response signaling and repair. Nucleic Acids Res. 2011;39(17):7465-76. doi:
882 10.1093/nar/gkr454.
883 41. Smith EA, Gole B, Willis NA, Soria R, Starnes LM, Krumpelbeck EF, et al. DEK
884 is required for homologous recombination repair of DNA breaks. Sci Rep.
885 2017;7:44662. Epub 2017/03/21. doi: 10.1038/srep44662.
886 42. Alexiadis V, Waldmann T, Andersen J, Mann M, Knippers R, Gruss C. The
887 protein encoded by the proto-oncogene DEK changes the topology of chromatin
888 and reduces the efficiency of DNA replication in a chromatin-specific manner.
889 Genes & development. 2000;14(11):1308-12.
890 43. Deutzmann A, Ganz M, Schonenberger F, Vervoorts J, Kappes F, Ferrando-May
891 E. The human oncoprotein and chromatin architectural factor DEK counteracts DNA
892 replication stress. Oncogene. 2014. doi: 10.1038/onc.2014.346.
893 44. Sirbu BM, Couch FB, Feigerle JT, Bhaskara S, Hiebert SW, Cortez D. Analysis
894 of protein dynamics at active, stalled, and collapsed replication forks. Genes &
895 development. 2011;25(12):1320-7. Epub 2011/06/21. doi: 10.1101/gad.2053211.

896 45. Merrick CJ, Jackson D, Diffley JFX. Visualization of Altered Replication
897 Dynamics after DNA Damage in Human Cells. Journal of Biological Chemistry.
898 2004;279(19):20067-75. doi: 10.1074/jbc.M400022200.
899 46. Schindelin J, Arganda-Carreras I, Frise E, Kaynig V, Longair M, Pietzsch T, et
900 al. Fiji: an open-source platform for biological-image analysis. Nat Meth.
901 2012;9(7):676-82.
902 47. Ball G, Demmerle J, Kaufmann R, Davis I, Dobbie IM, Schermelleh L. SIMcheck:
903 a Toolbox for Successful Super-resolution Structured Illumination Microscopy.
904 2015;5:15915. doi: 10.1038/srep15915.
905 48. Zheng L, Baumann U, Reymond JL. An efficient one-step site-directed and site-
906 saturation mutagenesis protocol. Nucleic Acids Res. 2004;32(14):e115. Epub
907 2004/08/12. doi: 10.1093/nar/gnh110.
908 49. Fahrer J, Kranaster R, Altmeyer M, Marx A, Burkle A. Quantitative analysis of
909 the binding affinity of poly(ADP-ribose) to specific binding proteins as a function of
910 chain length. Nucleic Acids Res. 2007;35(21):e143. Epub 2007/11/10. doi:
911 10.1093/nar/gkm944.
912 50. Gill SJ, Travers J, Pshenichnaya I, Kogera FA, Barthorpe S, Mironenko T, et al.
913 Combinations of PARP Inhibitors with Temozolomide Drive PARP1 Trapping and
914 Apoptosis in Ewing's Sarcoma. PLoS One. 2015;10(10):e0140988. Epub
915 2015/10/28. doi: 10.1371/journal.pone.0140988.
916 51. Velic D, Couturier AM, Ferreira MT, Rodrigue A, Poirier GG, Fleury F, et al. DNA
917 Damage Signalling and Repair Inhibitors: The Long-Sought-After Achilles' Heel of
918 Cancer. Biomolecules. 2015;5(4):3204-59. Epub 2015/11/28. doi:
919 10.3390/biom5043204.
920 52. Gustafsson MG, Shao L, Carlton PM, Wang CJ, Golubovskaya IN, Cande WZ,
921 et al. Three-dimensional resolution doubling in wide-field fluorescence microscopy
922 by structured illumination. Biophys J. 2008;94(12):4957-70. doi:
923 10.1529/biophysj.107.120345.
924 53. Rust MJ, Bates M, Zhuang X. Sub-diffraction-limit imaging by stochastic optical
925 reconstruction microscopy (STORM). Nature methods. 2006;3(10):793-5. doi:
926 10.1038/nmeth929.
927 54. Nozaki T, Imai R, Tanbo M, Nagashima R, Tamura S, Tani T, et al. Dynamic
928 Organization of Chromatin Domains Revealed by Super-Resolution Live-Cell
929 Imaging. Molecular cell. 2017;67(2):282-93 e7. doi: 10.1016/j.molcel.2017.06.018.
930 55. Ying S, Chen Z, Medhurst AL, Neal JA, Bao Z, Mortusewicz O, et al. DNA-PKcs
931 and PARP1 Bind to Unresected Stalled DNA Replication Forks Where They Recruit
932 XRCC1 to Mediate Repair. Cancer Res. 2016;76(5):1078-88. doi: 10.1158/0008-
933 5472.CAN-15-0608.
934 56. Toledo LI, Altmeyer M, Rask MB, Lukas C, Larsen DH, Povlsen LK, et al. ATR
935 prohibits replication catastrophe by preventing global exhaustion of RPA. Cell.
936 2013;155(5):1088-103. doi: 10.1016/j.cell.2013.10.043.
937 57. Maréchal A, Zou L. RPA-coated single-stranded DNA as a platform for post-
938 translational modifications in the DNA damage response. Cell Research.
939 2015;25(1):9-23. doi: 10.1038/cr.2014.147.
940 58. Bhat KP, Cortez D. RPA and RAD51: fork reversal, fork protection, and genome
941 stability. Nature structural & molecular biology. 2018;25(6):446-53. doi:
942 10.1038/s41594-018-0075-z.

943 59. de Murcia G, Jongstra-Bilen J, Ittel ME, Mandel P, Delain E. Poly(ADP-ribose)
944 polymerase auto-modification and interaction with DNA: electron microscopic
945 visualization. EMBO J. 1983;2(4):543-8. Epub 1983/01/01.
946 60. Brazda V, Laister RC, Jagelska EB, Arrowsmith C. Cruciform structures are a
947 common DNA feature important for regulating biological processes. BMC Mol Biol.
948 2011;12:33. Epub 2011/08/06. doi: 10.1186/1471-2199-12-33.
949 61. Salvati E, Scarsella M, Porru M, Rizzo A, Iachettini S, Tentori L, et al. PARP1 is
950 activated at telomeres upon G4 stabilization: possible target for telomere-based
951 therapy. Oncogene. 2010;29(47):6280-93. Epub 2010/08/31. doi:
952 10.1038/onc.2010.344.
953 62. Dungrawala H, Rose KL, Bhat KP, Mohni KN, Glick GG, Couch FB, et al. The
954 Replication Checkpoint Prevents Two Types of Fork Collapse without Regulating
955 Replisome Stability. Molecular cell. 2015;59(6):998-1010. doi:
956 10.1016/j.molcel.2015.07.030.
957 63. Lossaint G, Larroque M, Ribeyre C, Bec N, Larroque C, Decaillet C, et al.
958 FANCD2 binds MCM proteins and controls replisome function upon activation of s
959 phase checkpoint signaling. Molecular cell. 2013;51(5):678-90. Epub 2013/09/03.
960 doi: 10.1016/j.molcel.2013.07.023.
961 64. Ribeyre C, Zellweger R, Chauvin M, Bec N, Larroque C, Lopes M, et al. Nascent
962 DNA Proteomics Reveals a Chromatin Remodeler Required for Topoisomerase I
963 Loading at Replication Forks. Cell Reports. 2016;15(2):300-9.
964 65. Lopez-Contreras Andres J, Ruppen I, Nieto-Soler M, Murga M, Rodriguez-
965 Acebes S, Remeseiro S, et al. A Proteomic Characterization of Factors Enriched at
966 Nascent DNA Molecules. Cell Reports. 2013;3(4):1105-16.
967 66. Dantzer F, Santoro R. The expanding role of PARPs in the establishment and
968 maintenance of heterochromatin. FEBS J. 2013;280(15):3508-18. Epub
969 2013/06/05. doi: 10.1111/febs.12368.
970 67. Zhang Y, Wang J, Ding M, Yu Y. Site-specific characterization of the Asp- and
971 Glu-ADP-ribosylated proteome. Nature methods. 2013;10(10):981-4. doi:
972 10.1038/nmeth.2603.
973 68. Martello R, Leutert M, Jungmichel S, Bilan V, Larsen SC, Young C, et al.
974 Proteome-wide identification of the endogenous ADP-ribosylome of mammalian
975 cells and tissue. Nat Commun. 2016;7:12917. Epub 2016/10/01. doi:
976 10.1038/ncomms12917.
977 69. Bonfiglio JJ, Colby T, Matic I. Mass spectrometry for serine ADP-ribosylation?
978 Think o-glycosylation! Nucleic Acids Res. 2017. Epub 2017/05/19. doi:
979 10.1093/nar/gkx446.
980 70. Fischbach A, Kruger A, Hampp S, Assmann G, Rank L, Hufnagel M, et al. The
981 C-terminal domain of p53 orchestrates the interplay between non-covalent and
982 covalent poly(ADP-ribosyl)ation of p53 by PARP1. Nucleic Acids Res.
983 2018;46(2):804-22. doi: 10.1093/nar/gkx1205.
984 71. Illuzzi G, Fouquerel E, Ame JC, Noll A, Rehmet K, Nasheuer HP, et al. PARG is
985 dispensable for recovery from transient replicative stress but required to prevent
986 detrimental accumulation of poly(ADP-ribose) upon prolonged replicative stress.
987 Nucleic Acids Res. 2014;42(12):7776-92. Epub 2014/06/08. doi:
988 10.1093/nar/gku505.
989 72. Maya-Mendoza A, Moudry P, Merchut-Maya JM, Lee M, Strauss R, Bartek J.
990 High speed of fork progression induces DNA replication stress and genomic
991 instability. Nature. 2018;559(7713):279-84. doi: 10.1038/s41586-018-0261-5.

992 # SUPPORTING INFORMATION

993 **S1 Table** **Primer sequences for the site-directed mutagenesis of the DEK**
994 **primary sequence**

995 **S1 Fig.** **AZD-2281 but not ABT-888 induces DNA damage in U2-OS cells**

996 **S2 Fig.** **Absence of combined positive effect of DEK downregulation and**
997 **PARP1/2 inhibition on fork progression under high doses of HU**

998 **S3 Fig.** **HU-induced fork arrest**

999 **S4 Fig.** **Determination of RPA-positive cells**

1000 **S5 Fig.** **Mutational analysis of PBD1 and PBD3 using recombinant peptides**

1001 **S6 Fig.** **Reconstitution of U2-OS shDEK cells with DEK WT-GFP or DEK PBD2-**
1002 **Mut2-GFP**

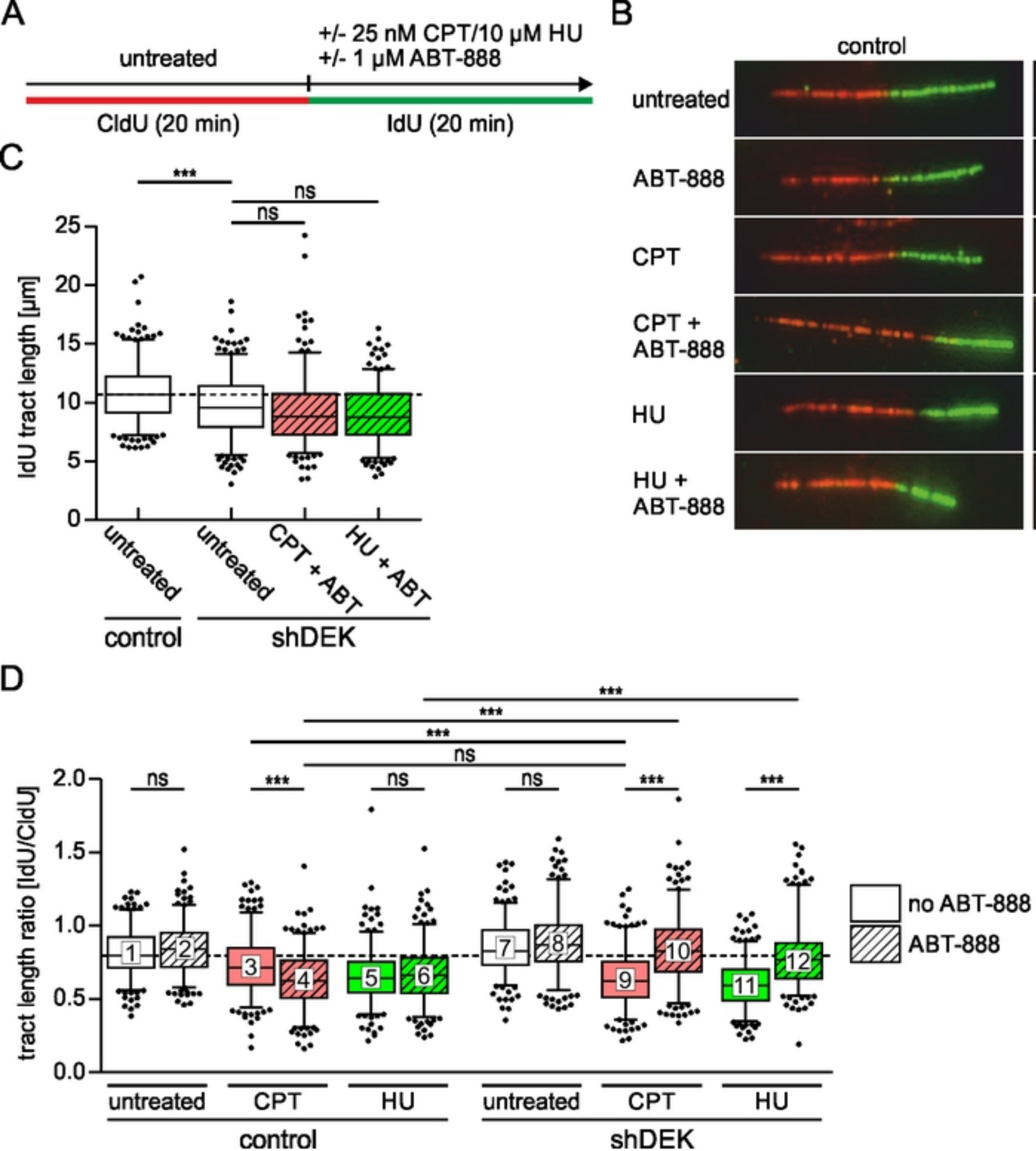
A
untreated
+/- 25 nM CPT/10 µM HU
+/- 1 µM ABT-888
CldU (20 min)
IdU (20 min)
B
control
shDEK
untreated
ABT-888
CPT
CPT + ABT-888
HU
HU + ABT-888
C
IdU tract length [µm]
untreated
untreated
CPT + ABT
HU + ABT
control
shDEK
D
tract length ratio [IdU/CldU]
untreated
CPT
HU
untreated
CPT
HU
control
shDEK
no ABT-888
ABT-888

Figure 1

A

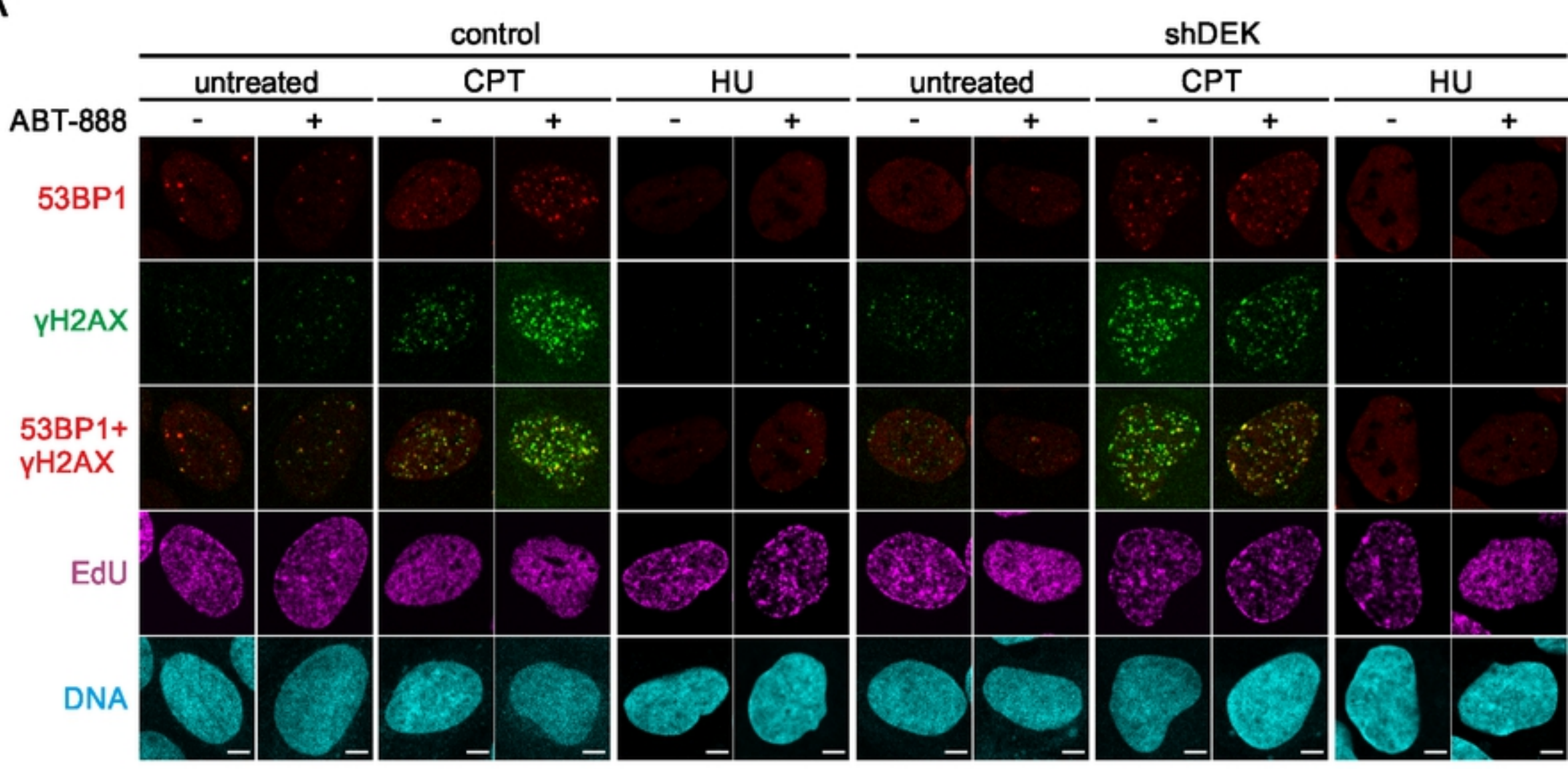
control
shDEK
untreated
CPT
HU
untreated
CPT
HU
ABT-888
-
+
-
+
-
+
-
+
-
+
-
+
53BP1
γH2AX
53BP1+
γH2AX
EdU
DNA

B

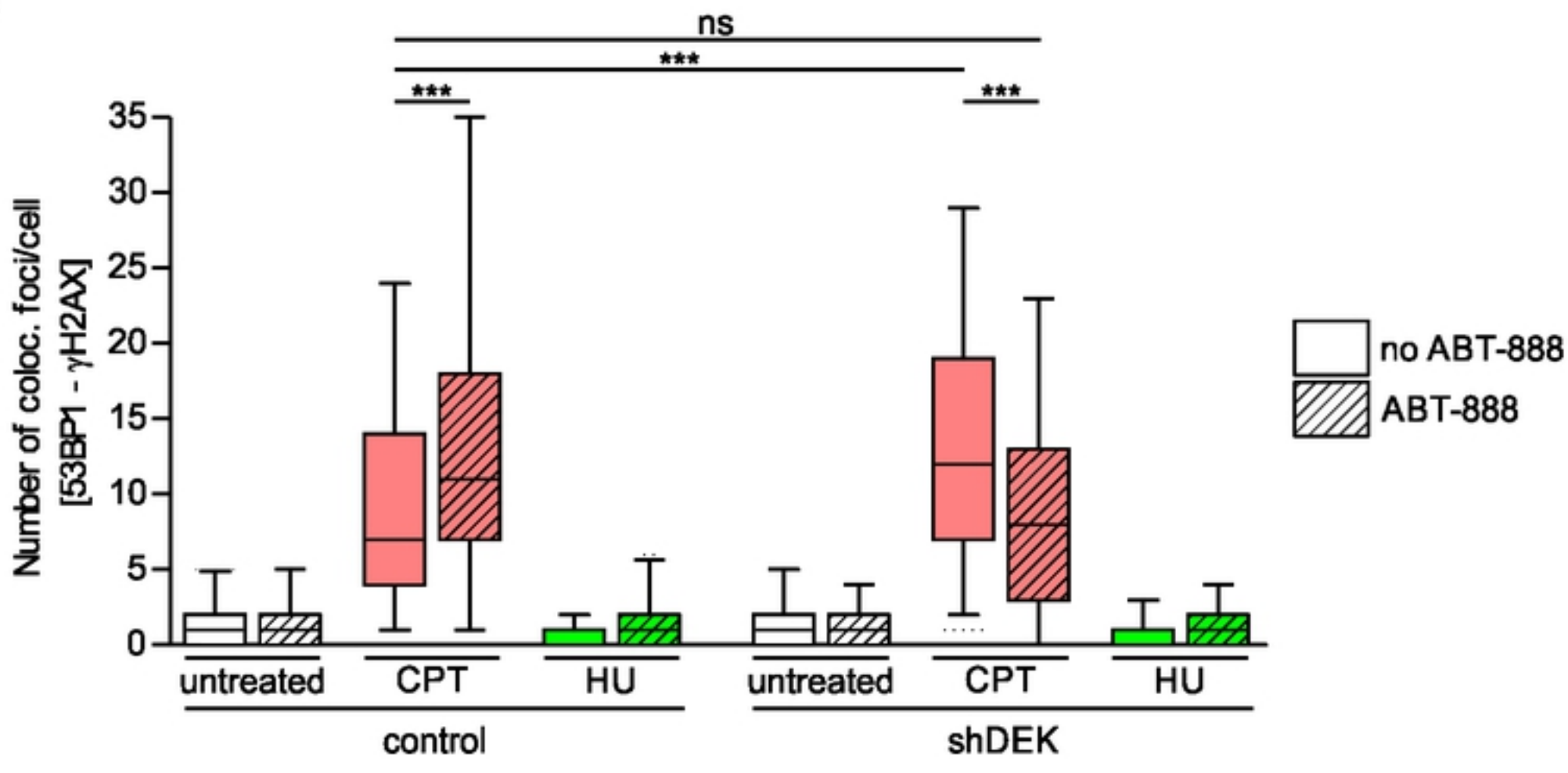
ns
***
***
***
Number of coloc. foci/cell
[53BP1 - γH2AX]
35
30
25
20
15
10
5
0
untreated
CPT
HU
untreated
CPT
HU
control
shDEK
no ABT-888
ABT-888

Figure 2

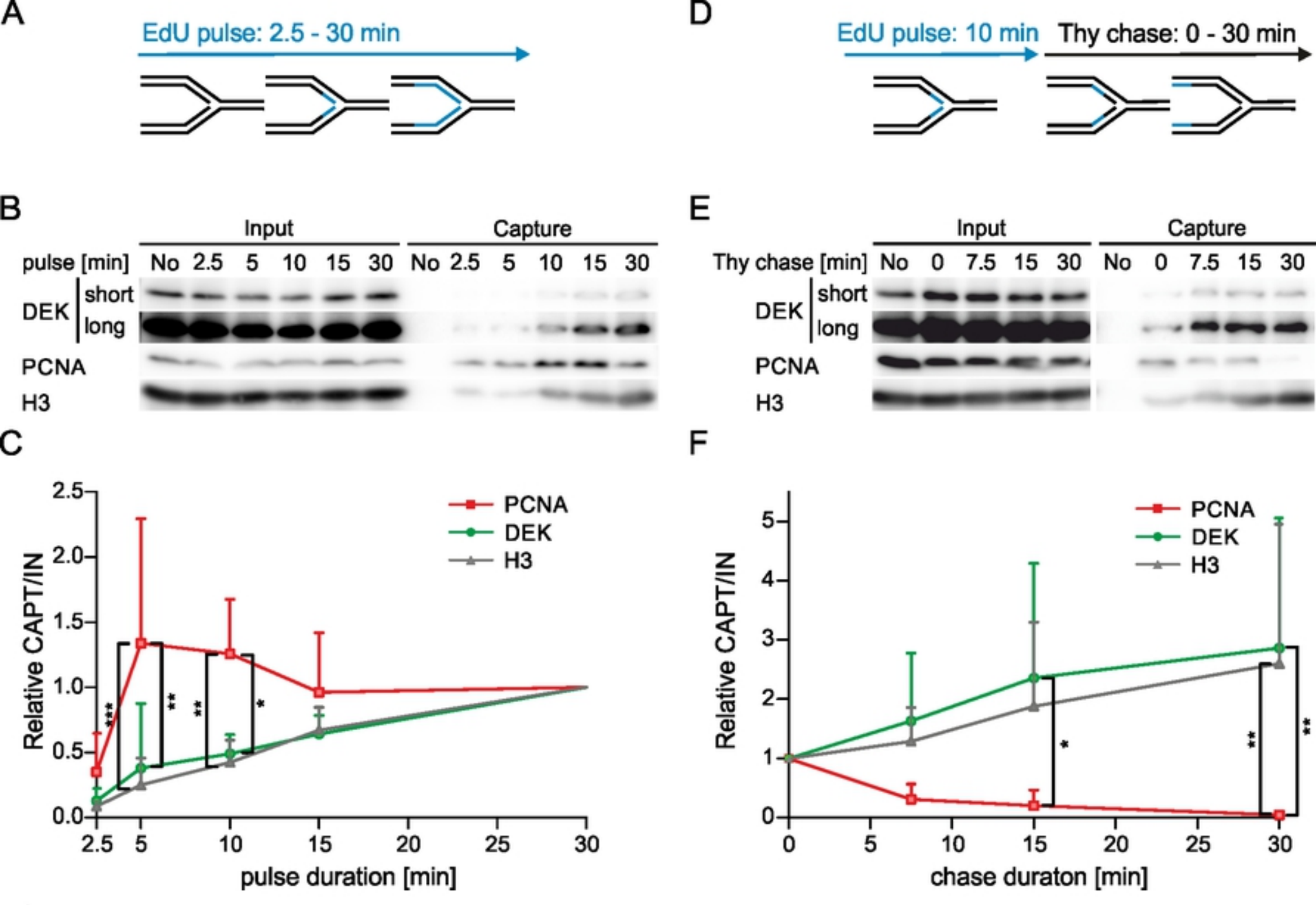
A
EdU pulse: 2.5 - 30 min
D
EdU pulse: 10 min
Thy chase: 0 - 30 min
B
Input
Capture
pulse [min]
No 2.5 5 10 15 30
No 2.5 5 10 15 30
DEK
short
long
PCNA
H3
E
Input
Capture
Thy chase [min]
No 0 7.5 15 30
No 0 7.5 15 30
DEK
short
long
PCNA
H3
C
Relative CAPT/IN
pulse duration [min]
PCNA
DEK
H3
F
Relative CAPT/IN
chase duraton [min]
PCNA
DEK
H3

Figure 3

A

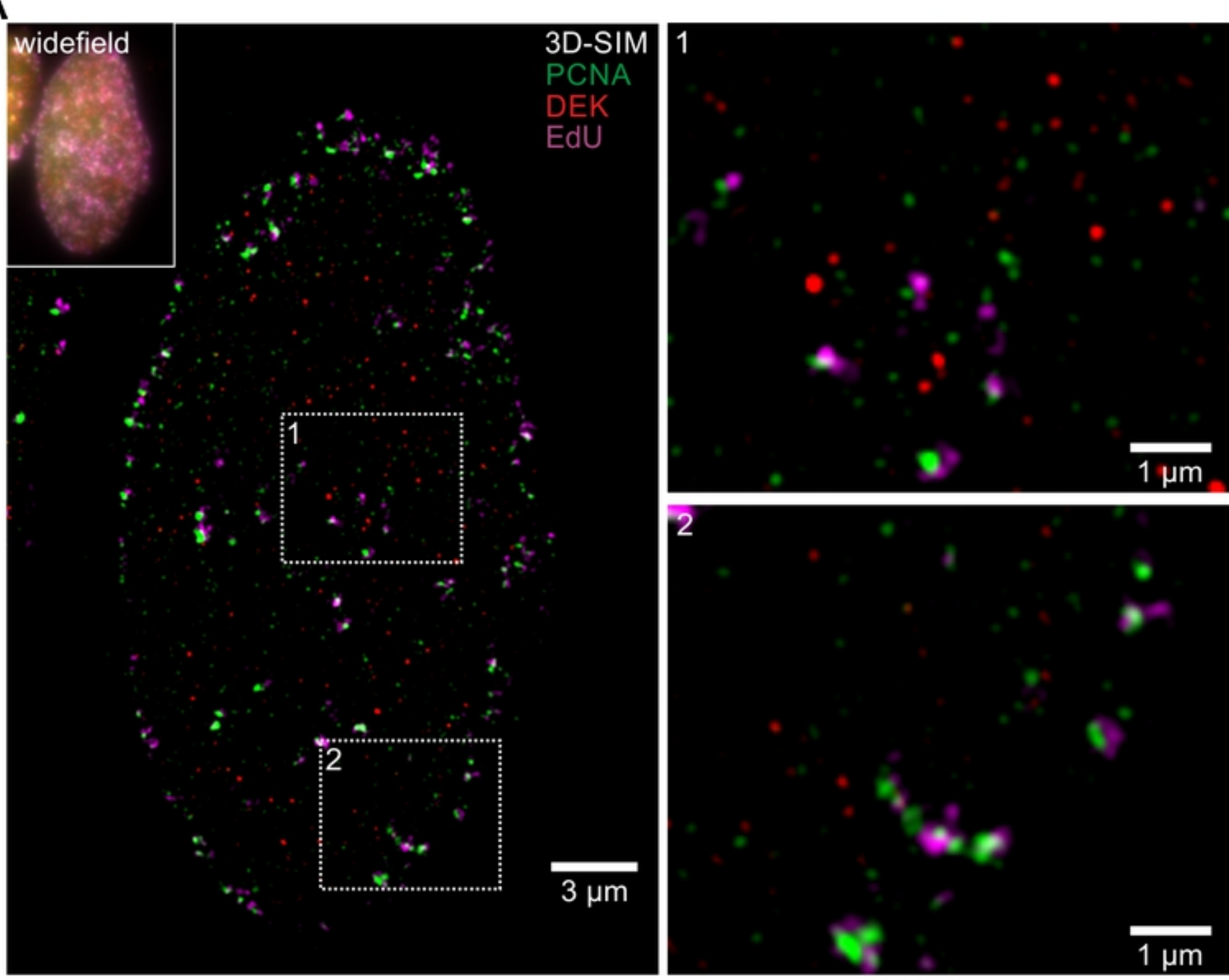
widefield
3D-SIM
PCNA
DEK
EdU
1
2
3 µm
1
1 µm
2
1 µm

B

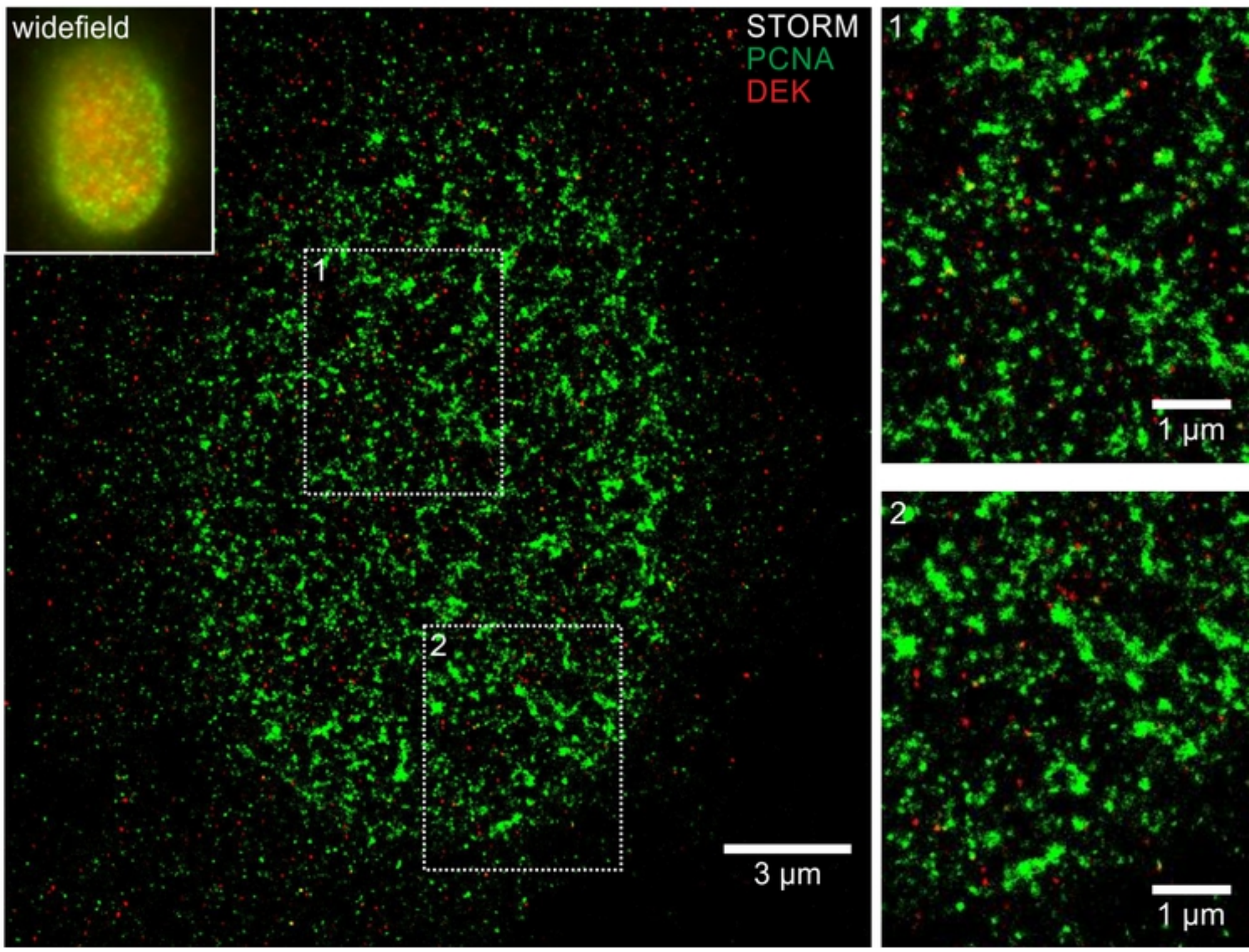
widefield
STORM
PCNA
DEK
1
2
3 µm
1
1 µm
2
1 µm

Figure 4

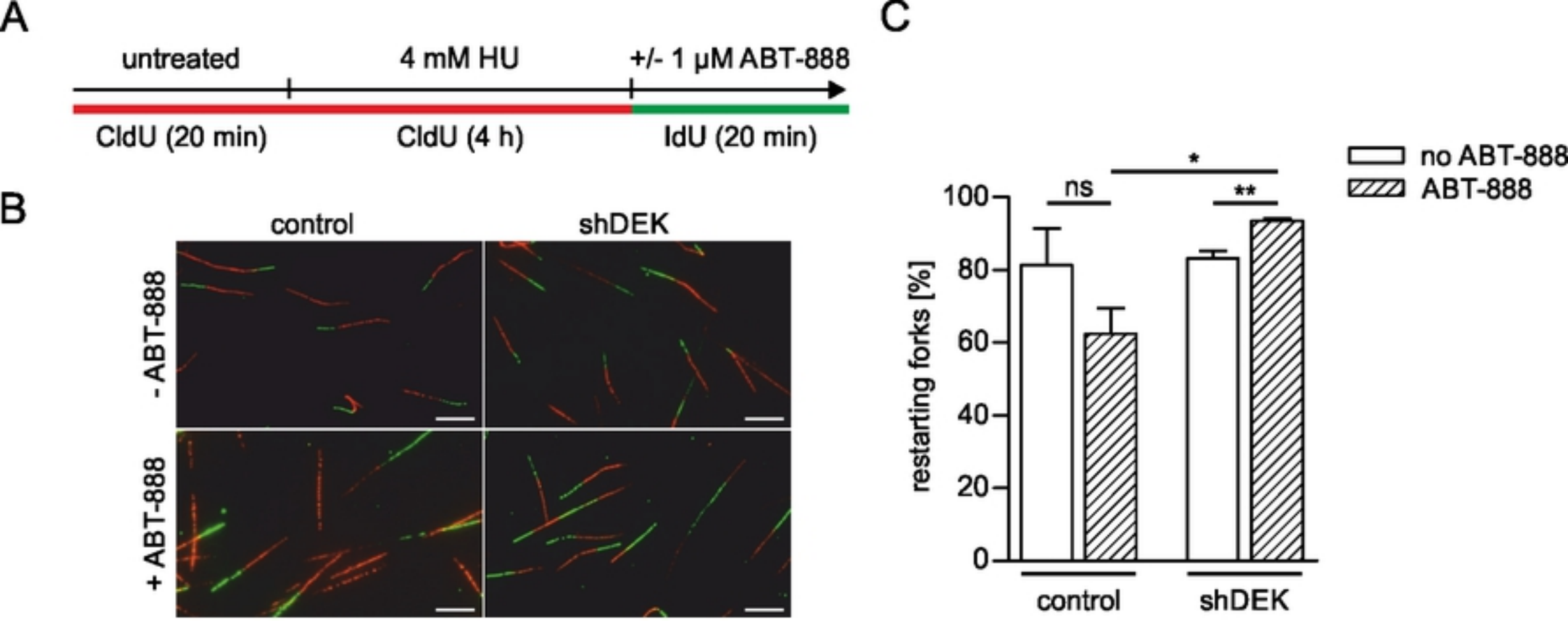
A
untreated
4 mM HU
+/- 1 µM ABT-888
CldU (20 min)
CldU (4 h)
IdU (20 min)
B
control
shDEK
- ABT-888
+ ABT-888
C
no ABT-888
ABT-888
ns
*
**
restarting forks [%]
100
80
60
40
20
0
control
shDEK

Figure 5

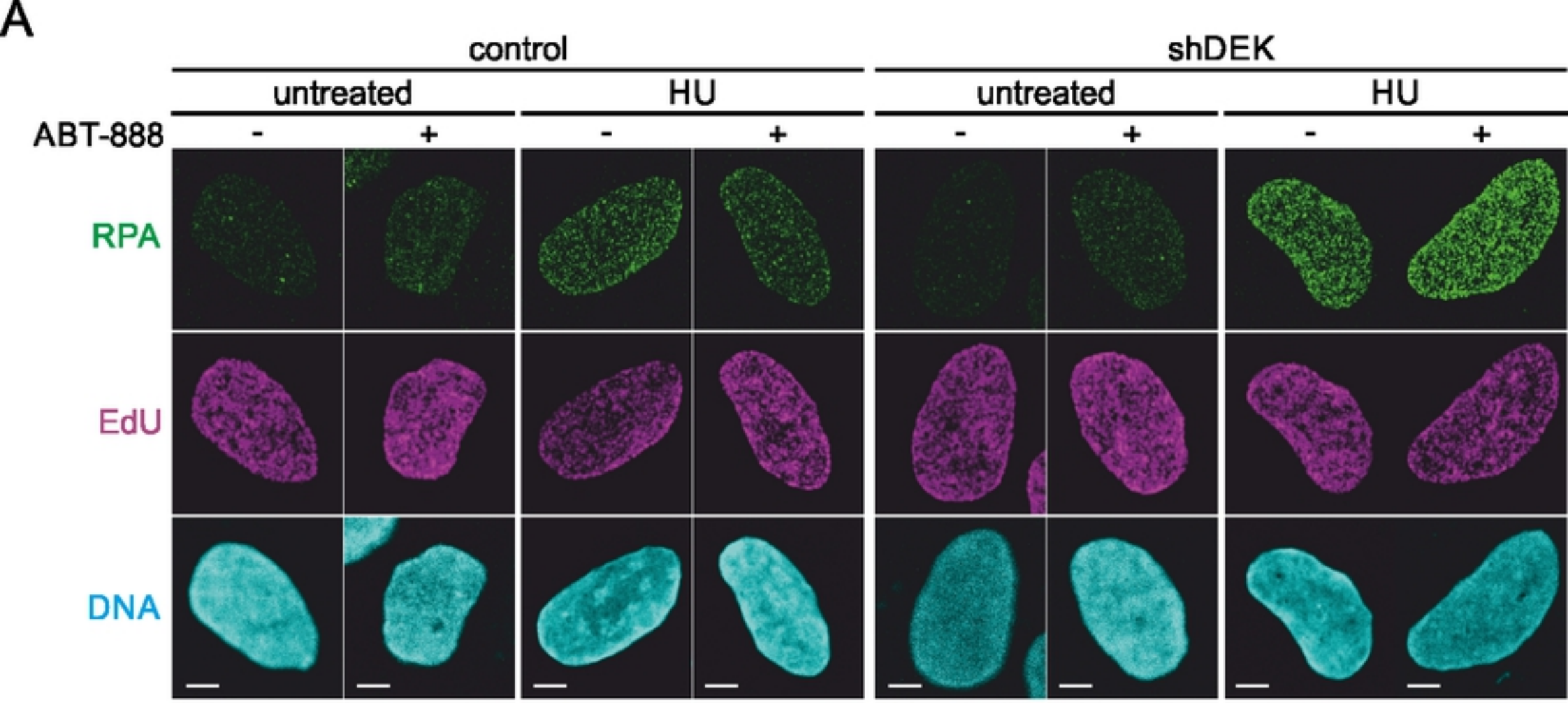
A
control
shDEK
untreated
HU
untreated
HU
ABT-888
-
+
-
+
-
+
-
+
RPA
EdU
DNA

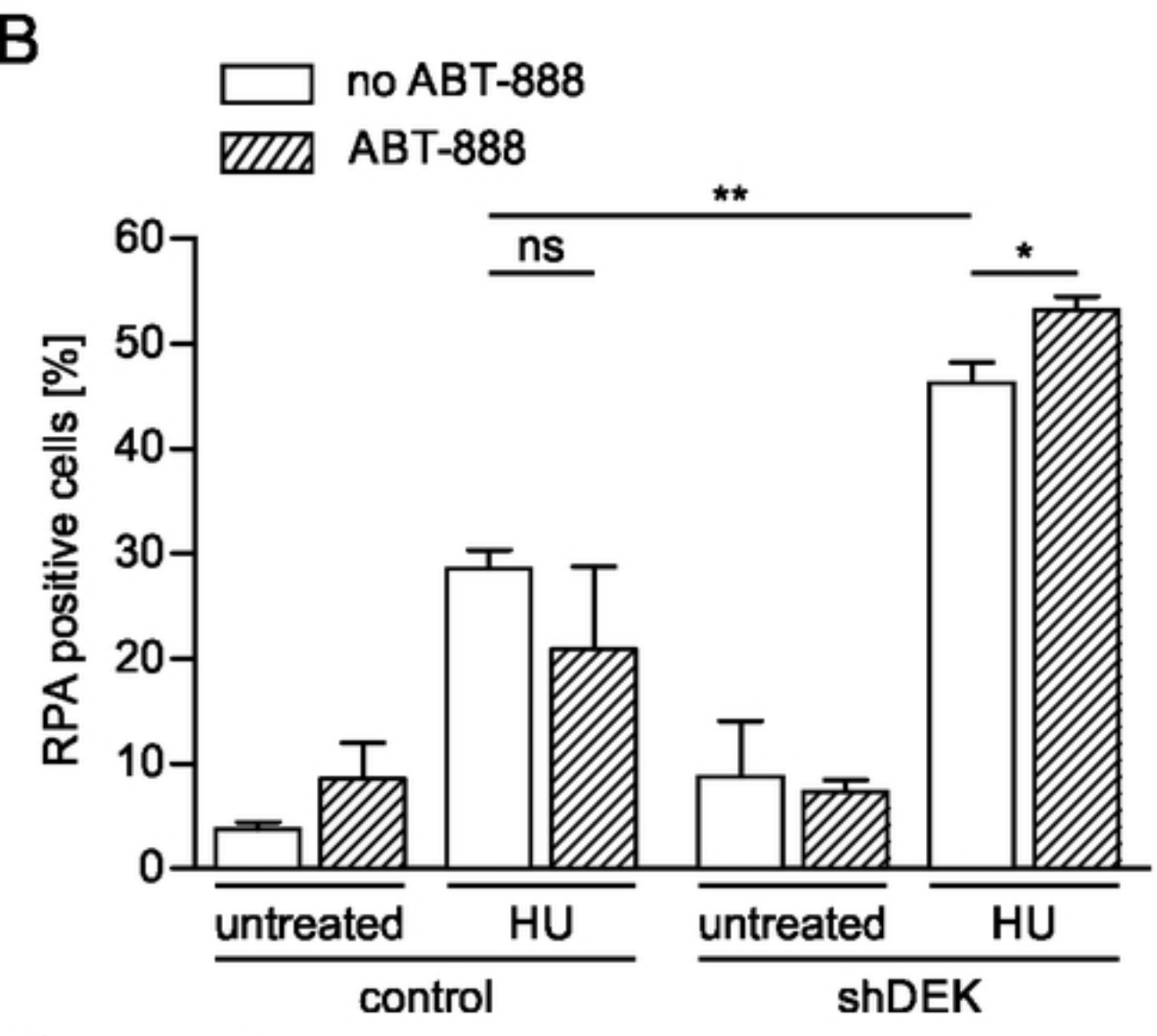
B
no ABT-888
ABT-888
**
ns
*
RPA positive cells [%]
60
50
40
30
20
10
0
untreated
HU
untreated
HU
control
shDEK

Figure 6

A

B

PBD2		basic stretch	core motif
DEK WT	195-222	KSKKTCSKGSKKE	RNSSGMARKAKRTK
DEK Mut1	195-222	KSKKTCSKGSKKE	RNSSGMAAAAAATA
DEK Mut2	195-222	KSAATCSKGSAAE	RNSSGMAAAAAATA
DEK Mut3	195-222	ASKKTCSAGSKKE	ANSSGMAAAAAATA
DEK Mut4	195-222	KSKKTCSKGSKKE	RNSSGAARKAKRTK

C

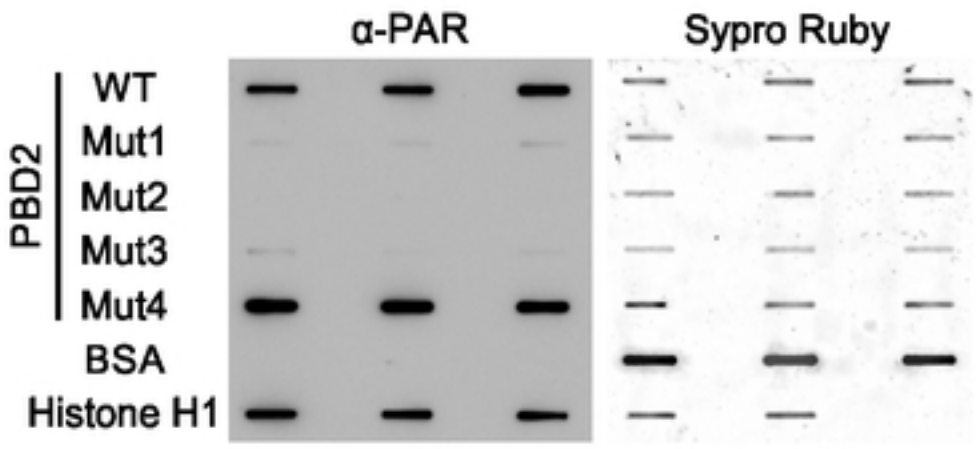

D

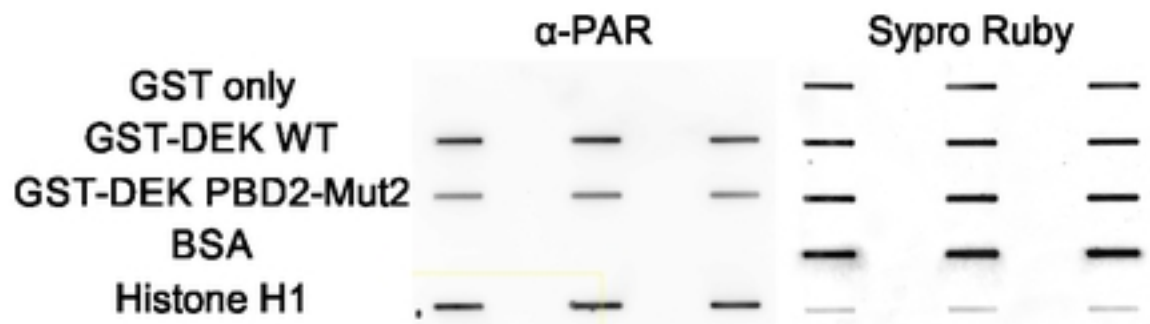

E

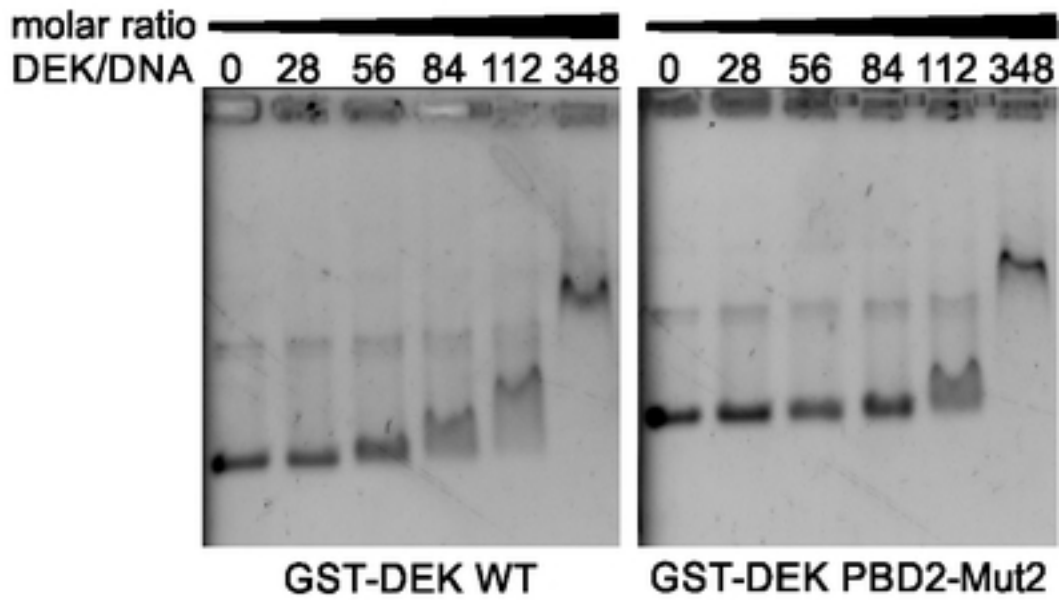

F

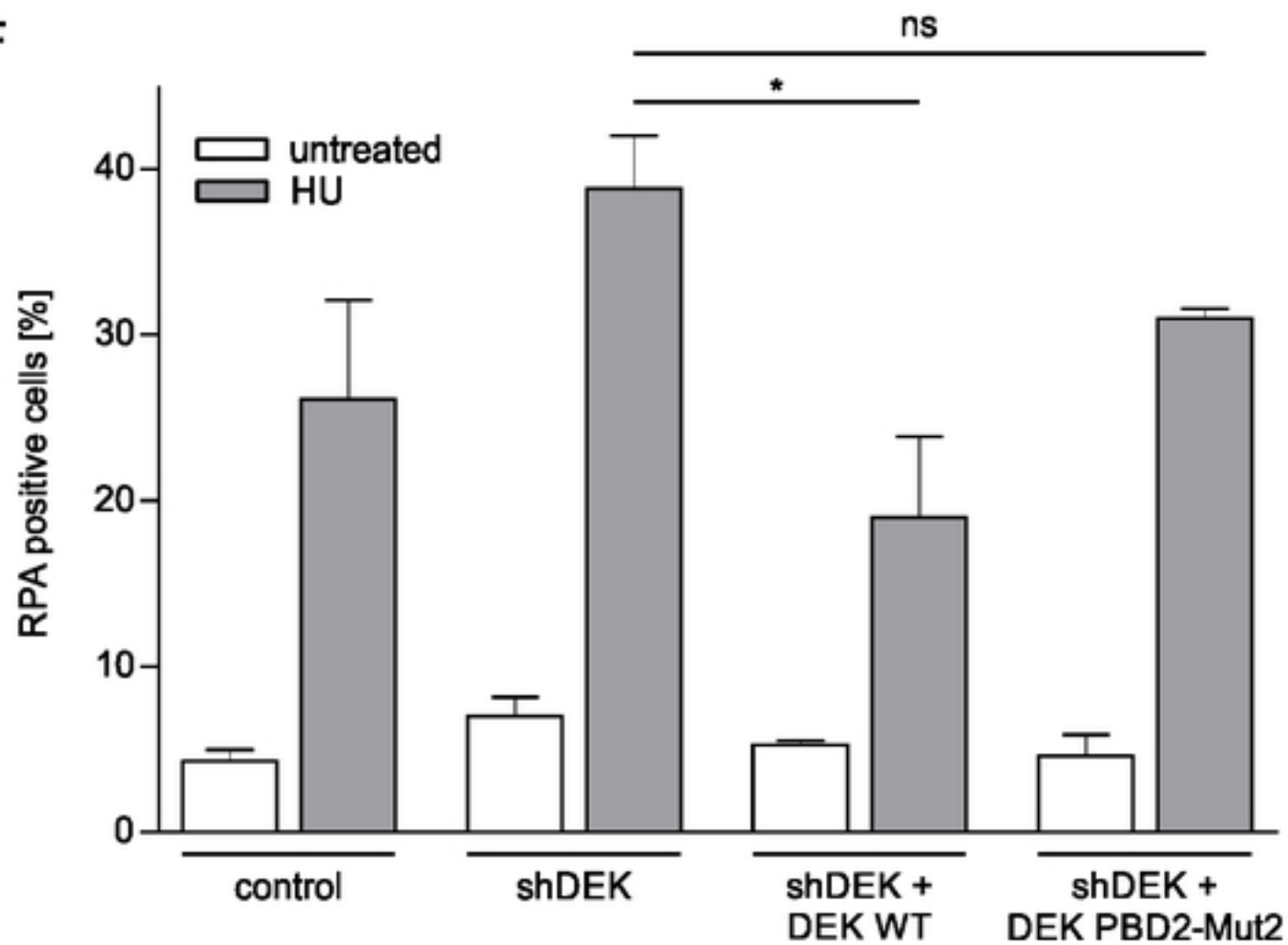

Figure 7